Chapter 5

Probing microarcsecond-scale structure using interstellar scintillation

The fault, dear Brutus, is not in our stars,
But in ourselves, that we are underlings.
Shakepeare's Cassius in *Julius Caesar*

5.1 Introduction

After the discovery of radio intraday variability (IDV) in extragalactic flat-spectrum sources (Heeschen, 1984), its origin was debated. Was the IDV intrinsic to the sources, implying excessively high brightness temperatures – 10^{21} K in the most extreme cases (Romero et al., 1994; Kedziora-Chudczer et al., 1997)? Or was the observed IDV caused by interstellar scintillation (ISS) (e.g. Rickett, 1990), and in this case, what were the implied brightness temperatures? The answers to these questions impact directly on the widely accepted model of incoherent synchrotron emission to explain the low-energy "hump" in the blazar spectral energy distribution (see Section 1.2).

While radio IDV had in some cases been successfully modelled as ISS (e.g. Rickett et al., 1995; Kedziora-Chudczer et al., 1997), an intrinsic origin was, until recently, favoured in the AGN community, based largely on an apparent correlation between radio and optical variations in S5 0716+714, observed in 1990 February (Quirrenbach et al., 1991; Wagner et al., 1996). However, from 1998, a great deal of evidence began to accumulate that ISS is in fact the principal mechanism for radio IDV. In late 1998, a significant time delay of ~ 2 minutes was observed between the IDV pattern arrival times at the ATCA and the VLA, for the extreme IDV source PKS 0405–385 (Jauncey et al., 2000a). In 2000, an "annual cycle" was detected in the characteristic variability time scales of the sources J1819+3845 (Dennett-Thorpe & de Bruyn, 2001) and 0917+624 (Rickett et al., 2001; Jauncey & Macquart, 2001). In addition, correlated IDV of circularly polarized and total flux density in PKS 1519−273 was explained as ISS by Macquart et al. (2000). Also around this time, new IDV sources

were being discovered as a result of the present ATCA long-term blazar monitoring program (Chapter 3) and other ATCA observations (see Section 5.2).

Observations of annual cycles in characteristic time-scales were recognised as a method of demonstrating unequivocally a scintillation origin of IDV. Furthermore, such annual cycles could potentially be used as a probe of microarcsecond (μas) source structure: "Earth Orbital Synthesis" (Macquart & Jauncey, 2002, ; see Section 1.3.7). Using ISS to constrain source sizes on scales of $\sim 10\mu$as potentially allows measurement of higher brightness temperatures than can be currently achieved with ground-based or space VLBI, which would help to decide whether or not the incoherent synchrotron model is acceptable.

For most known IDV sources, characteristic time-scales are on the order of a day, too long to measure the expected time delay, of order a few minutes, in pattern arrival times between two telescopes. Observations of annual cycles are therefore the most effective method of demonstrating ISS and probing μas-scale source structure. To this end, an ATCA proposal was submitted in October 2000 to monitor a number of known IDV sources over the course of a year, and the observational program commenced in early 2001. The sources were observed over 48-hour observing sessions, scheduled approximately every 6 weeks. This chapter describes the observational program (ATCA project C927) and presents first results from the program. The observations were set up to obtain measurements of both linear and circular polarization in addition to total flux density. Linear polarization results, and some circular polarization results, are presented here. This is a large project with a number of people involved, and data analysis is ongoing.

By far the most outstanding IDV source observed in the program was PKS 1257−326. This source displays extremely rapid IDV, which can be characterised reliably from a single, 12-hour observation. Hence, PKS 1257−326 became the focus of a detailed investigation. This source and the two other previously discovered rapid scintillators, PKS 0405−385 and J1819+3845, have been instrumental in making the "paradigm shift" to ISS as the principal mechanism for radio IDV, and in showing the value of ISS as a probe of microarcsecond-scale source structure and properties of the local ISM. Chapter 6 is devoted to the results from observations of PKS 1257−326 alone.

For the other IDV sources, which have significantly longer characteristic time-scales, large uncertainties are associated with estimating the time-scale of variability and other characteristics, from the 48 hour observing sessions. Results for some of the "slower" IDV sources observed are presented in Section 5.7.

5.2 The source sample

The sample for the ATCA IDV monitoring program, shown in Table 5.1, consists mainly of flat-spectrum sources already known to exhibit IDV. These include sources which showed strong IDV in the ATCA IDV Survey (Kedziora-Chudczer et al., 2001b) or in other studies or surveys (Quirrenbach et al., 1992; Kraus et al., 1999b; Romero et al., 1994). Several additional sources were included in which IDV had been recently

discovered with the ATCA, as described below. The ATCA IDV Survey found evidence to suggest that sources which are highly variable on long time-scales, and those with inverted radio spectra, are also those most likely to scintillate (Kedziora-Chudczer et al., 2001b). This result is not surprising as such sources are also generally the most core-dominated and compact. Therefore, some highly inverted spectrum sources and long-term variable sources found in the ATCA monitoring program for VSOP Survey sources (Tingay et al., 2003) were included as IDV candidates. At least 6 compact, non-IDV sources (see Table 2.1) were included in each session for calibration of changes in gain due to atmospheric and antenna-based effects, and for assessment of the level of errors. Three or more calibration sources known to have a few percent linear polarization were included in each session, as these are needed to solve the "strongly polarized" equations to measure circular polarization (Hamaker et al., 1996; Sault et al., 1996; Rayner, 2001). A number of other, slightly northern sources were observed only in some sessions to search for, or confirm, the presence of rapid variability. These included 3 rapid variable sources reported by Gorshkov & Konnikova (1996) and Gorshkov et al. (2000), and an optically rapid variable (C. Hazard, 2001, priv. comm.). These additional sources are also listed in Table 5.1, with footnotes indicating that these sources were not in the core sample.

New, strong IDV sources:

- IDV in PKS 1622−253 was discovered in the ATCA monitoring program described in Chapter 3.
- PMN J1047−6217 had been observed with the ATCA over a number of years as a phase calibrator and found to be extremely variable on timescales of weeks or less (S. White & R. Duncan 2000, private communication). In February 2001, the first session of the present monitoring program, this source showed strong IDV at 8.6 GHz.
- PMN J1326−5256 was observed with the ATCA during a search for suitable 22 GHz calibrators, and showed strong variability at 22, 8.6 and 4.8 GHz from observations two months apart (R.J. Sault 2001, private communication). The source has a highly inverted spectrum and is one of the brightest sources in the southern sky at 22 GHz. In January 2001, a change in flux density of $\sim 20-30\%$ at both 4.8 and 8.6 GHz was observed over 9 hours (Sault & Rayner, 2001, priv. comm.). In February 2001, the first session of the monitoring program, strong IDV was observed at both 4.8 and 8.6 GHz (see Section 5.7).
- ATCA data on PKS 1257−326 from 1995, which were re-examined in 2000, were suggestive of IDV in this source. Observations obtained with the ATCA during mid-2000 confirmed IDV in PKS 1257−326 (see Section 6.2). Subsequently, this source was found to show extremely rapid variability.
- PKS 1415−349 showed IDV in an ATCA Gravitational Lens Survey (Lovell, 1997, and priv. comm.).

5.3 The observations

The ATCA proposal requested observing sessions of 48 hours regularly spaced at intervals of approximately 6 weeks. Due to scheduling constraints for the array, and the large amount of time requested for this project (more than 400 hours in total), gaps between sessions were occasionally extended to 7–10 weeks, and sessions were sometimes broken up over 3 days. Some additional, shorter sessions were obtained to concentrate on PKS 1257−326, which was by far the most rapid variable, and required more frequent scans to obtain well-sampled light curves, compared with the other sources. A log of ATCA observations for this project is shown in Table 5.2.

The chosen observing frequencies were 4.8 and 8.6 GHz, for a number of reasons. Firstly, the break between strong and weak scattering in the ISM generally occurs at frequencies of a few GHz (e.g. Walker, 1998; Rickett, 2001b), so that characteristic timescales are significantly longer, of order days to weeks, at lower frequencies. Therefore it is usually not possible to estimate a characteristic variability time-scale at lower frequencies, from only two days of data. Secondly, the effect of confusion is more severe at lower frequencies. As the ATCA is a linear east-west array, the contribution of confusing sources varies with hour angle, and the effect of confusing sources must be subtracted from the visibilities. This complicates data analysis. Thirdly, another aim of the proposal was to investigate circular polarization in both IDV and non-IDV sources, to try to determine if there may be a link between scintillation and high levels of circular polarization (e.g. Macquart et al., 2000). Measurement of circular polarization with the ATCA is currently most accurate at 6 cm (Rayner, 2000). Circular polarization in AGN is usually weak ($< 0.5\%$), and careful calibration is required to avoid systematic errors. It was also desirable to avoid any systematic errors which may be introduced by rotating the ATCA antenna turrets during the observation. Calibration problems due to the turret not locking precisely into position after rotation, causing a change in feed alignment, were noted by Rayner (2000). Some circular polarization results are presented below in Section 5.6; further analysis of circular polarization data is to be presented elsewhere.

Each source, including calibrators, was observed for between 2 and 5 minutes approximately every hour while it was above 15° elevation. While the elevation limit of the ATCA is 12°, effects such as atmospheric opacity and pointing errors become significantly worse below about 15° elevation, which limits the level to which IDV can be reliably measured. Because of the rapid variability found in the source PKS 1257−326 (see Chapter 6), the time interval between observations of this source was decreased to $\sim$ 20–30 minutes where possible, except in the sessions concentrating on this source alone, where the sampling was almost continuous.

Full polarimetric calibration, using a calibration source of unknown polarization, requires good parallactic angle coverage. For a source which transits close to the zenith, most of the parallactic angle variation occurs near transit. The schedules were made to obtain more frequent cuts on polarization calibrators when they were near transit. This is most important for obtaining circular polarization, where it is necessary to solve the "strongly polarized" equations (Hamaker et al., 1996; Sault et al., 1996).

Table 5.1: IDV and candidate IDV sources observed in the ATCA C927 monitoring program. Footnotes refer to reported discovery of IDV or reason for including each source. The columns list the equatorial (J2000) and Galactic coordinates (l_{II}, b_{II}) for each source, and, where available, the redshift z and identification, 'ID'. In the 'ID' column, BL = BL Lac object, LBL = low-energy peaked BL Lac object, HBL = high-energy peaked BL Lac object, Q = quasar, HPQ = high optically polarized quasar.

Catalog name	RA (J2000)	Dec (J2000)	l_{II}	b_{II}	z	ID
PKS 0104−408[a]	01:06:45.11	−40:34:20.0	290.67	−76.19	0.584	LBL
AO 0235+164[b]	02:38:38.93	+16:36:59.3	156.77	−39.11	0.940	LBL
PKS 0346−279[c]	03:48:38.15	−27:49:13.3	224.53	−50.91	0.988	Q
PKS 0405−385[c]	04:06:59.04	−38:26:28.0	241.29	−47.89	1.285	Q
PKS 0502+049[d]	05:05:23.18	+04:59:42.7	195.48	−20.86	0.954	LBL
0506+056[d]	05:09:25.97	+05:41:35.3	195.41	−19.64	-	BL
PKS 0524+034[e]	05:27:32.71	+03:31:31.5	199.79	−16.85	-	LBL
PKS 0537−441[f]	05:38:50.36	−44:05:08.9	250.08	−31.09	0.894	LBL
PKS 1034−293[c]	10:37:16.08	−29:34:02.8	270.95	24.85	0.312	LBL
PMN J1047−6217[g]	10:47:42.95	−62:17:14.5	289.09	−2.79	-	-
PKS 1144−379[c]	11:47:01.37	−38:12:11.0	289.24	22.95	1.048	LBL
PKS 1257−326[h]	13:00:42.42	−32:53:12.2	305.18	29.94	1.256	Q
PMN J1326−5256[i]	13:26:49.20	−52:56:23.5	308.32	9.56	-	-
PKS 1415−349[j]	14:18:58.92	−35:09:42.4	322.48	24.37	-	-
PKS 1519−273[c]	15:22:37.68	−27:30:10.8	339.58	24.41	-	LBL
PKS 1622−253[h]	16:25:46.89	−25:27:38.3	352.14	16.32	0.786	Q
PKS 1622−297[c]	16:26:06.02	−29:51:27.0	348.82	13.32	0.815	Q
PKS 1921−293[k]	19:24:51.06	−29:14:30.1	9.34	−19.61	0.352	HPQ
PKS 1958−179[a]	20:00:57.09	−17:48:57.7	24.01	−23.12	0.65	HPQ
PKS 2155−304[c]	21:58:52.00	−30:13:32.3	17.73	−52.25	0.116	HBL
PKS 2201+171[l]	22:03:26.90	+17:25:48.0	75.67	−29.63	1.075	Q

[a] Inverted spectrum/long-term variable (Tingay et al., 2003)
[b] Kraus et al. (1999a)
[c] Found in ATCA IDV Survey (Kedziora-Chudczer, 1998; Kedziora-Chudczer et al., 2001b)
[d] Gorshkov & Konnikova (1996). Not in core sample.
[e] Gorshkov et al. (2000). Not in core sample.
[f] Romero et al. (1994)
[g] ATCA secondary calibrator (S. White & R. Duncan, priv. comm.)
[h] Discovered in ATCA data (this thesis)
[i] R. J. Sault, priv. comm.
[j] Showed IDV in ATCA gravitational lens survey (Lovell, 1997)
[k] High brightness temperature from VSOP (Hirabayashi et al., 2000)
[l] Optically highly variable (C. Hazard 2001, priv. comm.). Not in core sample.

Table 5.2: Log of observations for ATCA project C927. The columns headed $\mu_{\rm CAL}$ show the average percentage rms scatter in data on calibration sources at each frequency, 4.8 and 8.6 GHz.

Start date	Duration (h)	Notes	$\mu_{\rm CAL}$ (%)	
			4.8	8.6
2001-Feb-04	72	24 hours allocated to another project: observations combined	0.2	0.3
2001-Feb-28	5	PKS 1257−326: unallocated time		
2001-Mar-18	48		0.2	0.3
2001-Mar-23	9	ToO VLBI on PKS 1257−326		
2001-Apr-06	48		0.2	0.4
2001-Jun-02	43.5		0.2	0.4
2001-Jul-26	48	Bad weather—excluded in analysis	0.6	1.6
2001-Aug-04	14		0.3	0.4
2001-Aug-11	12		0.2	0.2
2001-Aug-30	12	Concentrated on PKS 0405−385		
2001-Sep-20	48		0.3	0.5
2001-Nov-03	6	PKS 1257−326		
2001-Nov-24	6	PKS 1257−326		
2001-Nov-29	47		0.2	0.3
2002-Jan-04	48		0.2	0.6
2002-Feb-22	48	Reduced source list		
2002-Apr-13	20	3 sources		

Finally, sources were offset from the array phase centre to ensure any artefacts due to 'DC' terms in the correlator output would not corrupt an image of a source. While correlator DC terms are rarely a problem for the ATCA, offsetting sources from the phase centre is another procedure recommended by Rayner (2001) for circular polarization observations. However, it is also important to observe sources at the pointing centre so that errors due to the primary beam polarization response are avoided. At the ATCA, there is not a simple way to offset the phase centre from the pointing centre, so the usual procedure is to add a small offset of, say, $20''$ to the source coordinates in the schedule, then add a corresponding pointing centre offset to the schedule, to move the primary beam centre away from the phase centre and onto the source.

5.4 Data reduction

As was the case for the data presented in Chapter 3, the MIRIAD software package was used for data reduction. However, some different steps were taken to optimise the calibration for studies of intraday variability. The flow-chart in Figure 5.1 summarises the steps involved.

The MIRIAD task TRANSFIX corrects for polarization leakage caused by errors in the ATCA antenna orientation, which occurs most strongly near transit (Kesteven, 1997). TRANSFIX requires input from the table of antenna pointing parameters, which are redetermined after each array reconfiguration and stored in an electronic log file at the ATCA. Task UVEDIT is then applied to artificially move sources back to the phase centre, since the calibration task GPCAL assumes the source has been observed at the phase centre. This procedure will also move any correlator DC artefact, so the original purpose of observing sources away from the phase centre is not lost. For all 8.6 GHz data, the elevation-dependent corrections derived in Section 2.3.5 were applied. Data were edited where necessary, as described in Section 3.2.3. The next step is to solve for bandpass and polarization leakages. For circular polarization measurements, it is important to solve the "strongly polarized" equations (Sault et al., 1996), and this has been done for some epochs following the steps described by Rayner (2001). For linear polarization measurements only, it is sufficient to find the leakage corrections using a weakly polarized source, and PKS 1934−638, which was observed in every session, typically every ~ 2 hours while above 15° elevation, was used for this purpose.

Time-dependent antenna gain corrections, which usually vary by $\lesssim 1\%$ over an observation, were then derived at both frequencies, from the calibration source observations. These gain solutions were merged and averaged to find an amplitude gain correction for each antenna every 30-60 minutes. These corrections were then applied to all sources with simple linear interpolation. Phase self-calibration was then performed on all sources, using a point-source model and setting the solution interval to a single, 10-second integration, as all sources observed are strong and point-like at the ATCA, and using a short solution interval ensures no decorrelation due to poor atmospheric phase stability. In some cases where a source contains some flux density in extended components, these were modelled and subtracted from the visibilities as

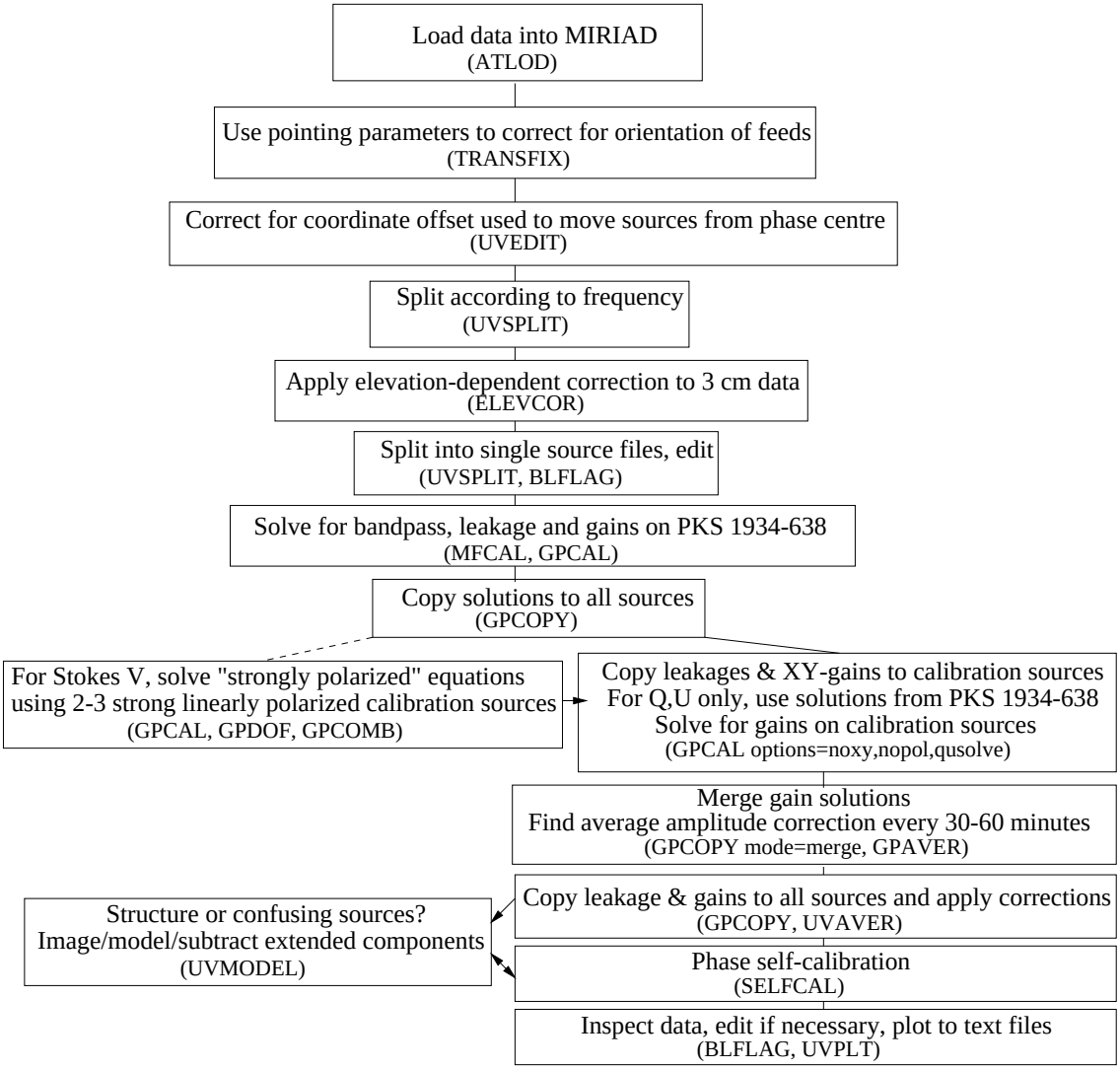

Figure 5.1: Reduction procedure in MIRIAD for data from ATCA project C927.

described in Section 5.4.2. The real parts of the visibilities of Stokes I, Q and U were then written out for analysis, using averaging intervals ranging from 1 to 5 minutes.

5.4.1 Flux density and polarization measurement errors

There are three main sources of error for the ATCA which affect IDV measurements: thermal noise, proportional gain errors, and variations with hour angle due to structure and confusion. Also, for polarization measurements, errors in the determination of leakage and the relative gains of the X and Y polarization channels contribute to the total error budget.

For a 1-minute integration with the ATCA, the thermal noise is ~ 1 mJy. All of the observed sources are stronger than 100 mJy in total intensity, and the total intensity measurement accuracy is never limited by the thermal noise. Measurements of Stokes Q, U, and V, however, may be limited by the thermal noise as the signal in polarized flux density is generally much weaker than for total intensity. Stokes Q and U were averaged over each scan, but as each scan was only 2-5 minutes in duration, the thermal noise is $\gtrsim 0.5$ mJy.

Errors in the measured fractional linear polarization due to uncertainties in leakages and X/Y gains are estimated, from the observed rms scatter for assumed non-variable calibration sources, to be typically $\sigma_p/I \sim 0.1\%$. Where the calibration for Stokes V has been performed, it is estimated to be accurate to $\sigma_V/I \sim 0.01\%$, based on a comparison of average values of V in three different sessions (so far, only average values of V in each of these sessions have been computed). Measurements of variability in Stokes V within each session are generally limited by signal-to-noise. Further analysis of Stokes V data is ongoing.

Table 5.2 shows the average rms scatter in each session for total flux density measurements of the calibration sources, $\mu_{\rm CAL}$. These values indicate the level of proportional errors in the data, but since hourly averaged gain corrections for each antenna have been derived from the calibration sources themselves, the errors may be slightly underestimated. Allowing for this, the rms proportional error for total flux density measurements is still less than 1% in good weather. Bad weather may significantly increase the errors. It is therefore important to compare the level of variation in data on non-IDV calibration sources, with the variation observed for the target sources. Proportional errors are the dominant source of error for total intensity measurements in the case of an isolated point source.

All observed sources are strongly core-dominated. For some sources, however, total flux density measurement uncertainties are dominated by weak extended structure or confusing sources in the field. In this case, subtraction of the extended components from the visibilities has been attempted, as described below. The contribution from extended structure changes with hour angle and with baseline, and the effect tends to be smoothed out to a large extent by averaging over all baselines. The level of variation due to extended structure can be estimated from the closure phases (see Section 2.2.4) or from plots of visibilities as a function of distance in the (u, v) plane.

5.4.2 Subtraction of extended components from the visibility data

The presence of extended emission and confusing sources in the field is an important concern for IDV studies. Usually, visibilities are plotted averaged over all baselines to determine IDV parameters. However, if a source has detectable structure, then after such averaging it is not possible to separate the effects of structure and variability in the visibilities, except that the rms scatter in the data will be somewhat larger than the theoretical rms for a point source. One of the reasons for choosing the observing frequencies of 4.8 and 8.6 GHz is that there is generally little confusion at these frequencies. For a few sources, however, significant structure or confusion is present at the observed frequencies, which if not subtracted limits the level to which IDV can be measured. If the extended emission and/or confusing sources are well-modelled, then their effects can be subtracted from the visibilities.

A problem arises when trying to image rapidly variable sources, as variability causes artefacts in the image (see for example Lecture 17 of TCP99, by W. D. Cotton). This problem is hard to deal with in data from a linear array such as the ATCA, compared with, for example, VLA data which has better, two-dimensional, instantaneous (u, v) coverage. The configuration of the VLA allows reasonable imaging from a single snapshot, whereas the instantaneous (u, v) coverage of the ATCA is linear. Thus, an image produced from a single ATCA scan does not give two-dimensional information; at a different hour angle, the contribution of extended structure will be quite different. However, for most sources observed, there are some datasets in which the source shows very little variability over a 12-hour period, and in this case it is possible to make an image which is free of artefacts due to amplitude "errors" introduced by variability. Assuming that the extended structure and confusing sources do not vary significantly over a given period, then the same model can be used at different epochs within that period.

For three sources in the ATCA sample which contain significant extended emission, an image was produced using data from a day where the source showed little variability. The MIRIAD task UVMODEL was then used to subtract the model CLEAN components from the data for all epochs, bar the central, unresolved source component. It was assumed that the model could be applied to all epochs over the year of the observations, i.e. (i) that the extended emission in the field did not vary significantly over a 12 month period, and (ii) that any variation in sampling due to different array configurations in different epochs did not have a significant effect on the model. In all observed cases, extended and confusing emission has an optically thin spectrum making it unlikely to be variable, therefore assumption (i) is probably reasonable. The various array configurations often have very different short spacings and are therefore sensitive to different angular scales, which affects assumption (ii) to some extent. Where necessary, data on the shortest baselines were discarded to remove the contribution of any residual, diffuse emission.

Ideally, one could use an iterative procedure for every dataset of modelling a time-variable point source, subtracting this and imaging the extended structure, then sub-

tracting the extended structure to obtain a better model of the time-variable source and so on until a good model for both variable source and extended structure is obtained. This procedure is time-consuming, however, and not necessary for the sources observed here, which have low levels of extended structure and confusion. For the IDV sources examined in detail here, the observed variability is much greater than the uncertainties in the unresolved component flux density due to residual structure or gain variations.

PKS 1144−379 has a relatively strong confusing source ~ 2.4 arcmin away, which is point-like with flux density ~ 40 mJy at 4.8 GHz, and ~ 25 mJy at 8.6 GHz. Such an optically-thin spectrum source is unlikely to itself be variable. The secondary source produces rapid fluctuations in the Stokes I visibilities as it "beats" with PKS 1144−379. A model of the confusing source has been subtracted from all 4.8 GHz data, which significantly reduces the rms scatter in the visibilities (see Figure 5.2). The large-amplitude, 1–2 day time-scale variability displayed by PKS 1144−379 can, however, be clearly observed in either case.

Another method of analysis for IDV sources where the field contains relatively simple structure, is to split the data into separate, short time intervals, and use a model-fitting procedure to constrain the flux density of the components in each interval. This technique was used for a VSOP observation of PKS 0405−385 during a period of rapid variability (J.E.J. Lovell, priv. comm.). For the case of PKS 1144-379, a simple two-component model-fit was tested in the same way. Allowing the flux densities of each component to vary, scan-by-scan flux densities for both components were obtained. The MODELFIT task in the Difmap software package (Shepherd, 1997) was used for this purpose. The results of the model-fit showed that the central source component varied, while the flux density of the confusing source remained constant within a few mJy. The model-fitting procedure is somewhat more time consuming than subtraction using UVMODEL in MIRIAD. Also, there appears to be other confusing sources near PKS 1144-379 which have a lesser, but detectable, effect on the visibilities. A practical limit of $\sim 4\%$ peak-to-peak variation is taken as the level to which IDV can be reliably measured for PKS 1144-379. The variations of $\sim 15\%$ peak-to-peak which are typically observed in this source remain highly significant.

PKS 1622−253 contains a compact jet (see Figure 3.2), which has been modelled as a set of CLEAN components at both frequencies, and subtracted from the visibilities. Figure 5.3 shows (u, v) data for PKS 1622−253 at 4.8 GHz before and after subtraction of the extended structure. While some residual structure remains, most of the extended emission has been removed from the visibilities. The difference in flux density over two consecutive days, due to the slow IDV of PKS 1622−253, can be seen clearly in this figure.

PKS 2155−304 has an extended halo (e.g. Pesce et al., 1997), which has been subtracted from the visibilities.

PKS 1257−326 also has weak extended structure, which was difficult to model in ATCA data due to the extremely rapid, large-amplitude variability of the source. Data from a VLA observation (see Section 6.3) has been used to produce high dynamic range images. For most of the ATCA data, the model of the PKS 1257−326 jet has not yet been subtracted from the visibilities, but this has little effect on the any of the results

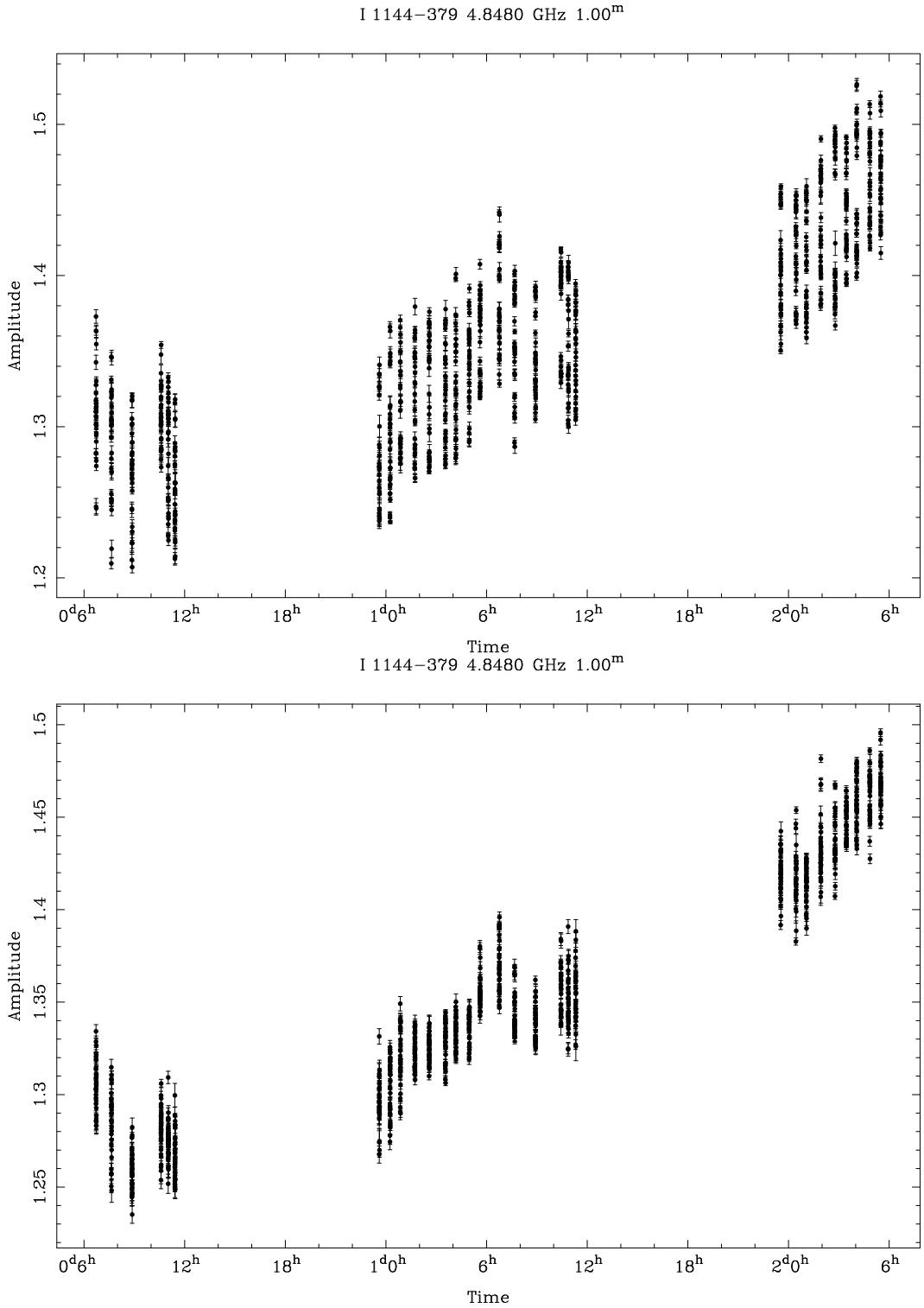

Figure 5.2: 48 hours of data on PKS 1144−379 at 4.8 GHz from 2001 July 26-27, before (above) and after (below) subtraction of the strongest confusing source in the field. Data are averaged over 1 minute, with separate points showing the amplitude of Stokes I measured on each baseline, plotted as a function of time.

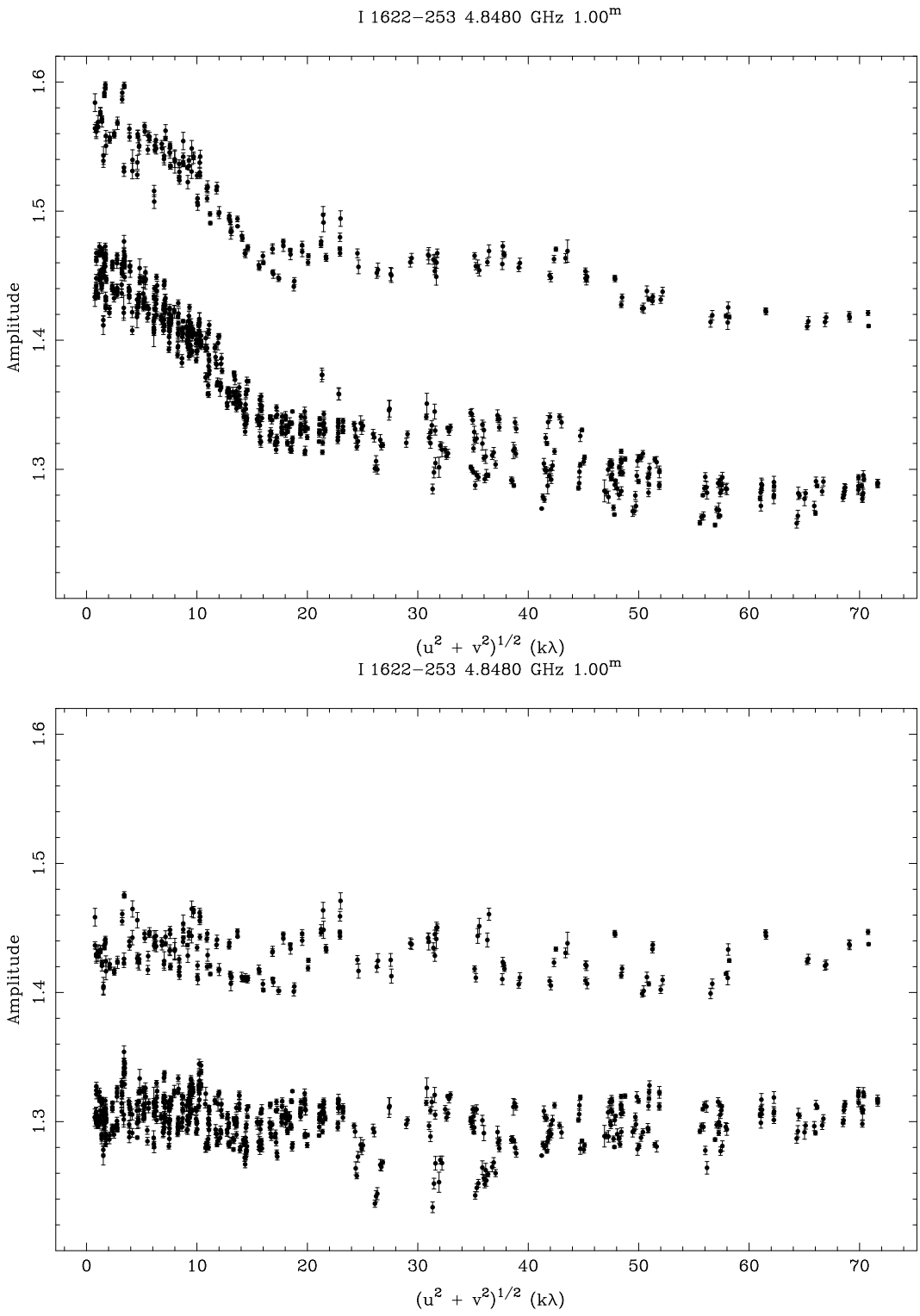

Figure 5.3: Data from 2001 March 17-19 on PKS 1622−253, before (above) and after (below) subtraction of modelled jet component. The amplitude of Stokes I from the visibilities, averaged separately for each baseline over 1-minute integrations, is plotted as a function of distance in the (u, v) plane. A large gap separates two days of data, due to IDV in the source, which is not sampled for the 12-hour periods when the source is below the horizon.

presented, as discussed in Section 6.3.3.

5.5 Analysis

As for the long-term variability analysed in Chapter 4, IDV is characterised by a time-scale and amplitude of variability. In the case of scintillation, the time-scale of variability relates to both the length scale of the scintillation pattern, and the speed at which this pattern moves past the observer. The amplitude of variability depends on the amount of the source flux density in the scintillating component(s), the angular size of the source, and the observed frequency; more specifically, on the ratio of the observed frequency to the transition frequency between weak and strong scattering (e.g. Walker, 1998).

The modulation index, defined in Section 4.2.1 as the fractional rms variation, $\mu = \sigma_S/\bar{S}$, is used as a measure of variability, and in estimating the level of flux density measurement errors from the calibration source data. The modulation index for Stokes I, corresponding to total flux density, has been calculated for all observed sources in all epochs.

For Stokes Q and U, corresponding to linearly polarized flux density, signal-to-noise for short scans is generally much lower than for Stokes I, and in this case, fractional variability is not meaningful. The modulation index can be very large, simply because the total polarized flux density is close to the level of the rms scatter due to thermal noise. Therefore, the un-normalized rms variations, in mJy, observed in Stokes Q and U, are used as a measure of IDV in linear polarization.

5.5.1 Limits on detectable variability

As a first cut, a conservative approach is taken to decide whether a source is variable within an observing session or not. Sources with a total flux density modulation index larger than 2% are deemed to be variable. The $\mu_I > 2\%$ cutoff is well above the modulation indices of all calibration sources, and is larger than any estimated rms variation due to unsubtracted structure. Since all sources have $I \geq 0.2\,\mathrm{Jy}$, the rms scatter due to thermal noise for each measurement, which is $< 1\,\mathrm{mJy}$, contributes $\mu_I < 0.5\%$ in all cases, and for most sources is completely negligible.

To decide which sources are variable in Stokes Q and U, a slightly more careful approach is required, since for some strong sources, leakage and XY-gain errors are significant. For the calibration sources, σ_Q/I and σ_U/I are typically no larger than 0.1%. Taking all sources of error into account, the conservative criterion for a source to be considered variable in Stokes Q, or U, is chosen to be

$$\sigma_Q > \sqrt{(1)^2 + (0.02Q)^2 + (0.003I)^2}\,\mathrm{mJy}. \tag{5.1}$$

The same limits for Stokes I, Q and U variability are used also to classify the long-term variability of a source over the whole year of observations.

A substantial fraction of flat-spectrum sources have been found to "flicker" at cm wavelengths, with typical amplitudes of a few percent, on time-scales of 2–20 days, while a smaller fraction show more rapid, larger-amplitude variability (Heeschen, 1984; Heeschen et al., 1987; Quirrenbach et al., 1992). It is the latter class of sources that is of most interest here; in particular, those sources whose time-scales can be characterised from a 48 hour observation. Most of the target sources show larger modulation indices than the calibration sources, but not all have been deemed to be "variable" using the above selection criteria (see Section 5.6). Only the most variable sources have been examined in detail so far. The sample was deliberately selected to contain the strongest IDV sources known - the statistics of the sample as a whole are not meaningful. A large IDV Survey has been recently undertaken with the VLA (Lovell et al., 2002, 2003, see Chapter 7), in order to investigate the statistics of IDV in a large, well-defined sample of flat spectrum radio sources.

5.5.2 Defining the characteristic time-scale of variability

Various authors have used different definitions for the characteristic time-scale of IDV sources. These are generally based upon estimates of either the auto-correlation function (ACF) or the structure function of the time series, or may be estimated from the time series itself. In studies of scintillation of pulsars, the usual convention is to define the time-scale as the lag at which the ACF falls to $1/e$ of its maximum value (Cordes, 1986). This definition of the "decorrelation time-scale", $t_{\rm dc}$, was adopted by Macquart & Jauncey (2002) in their paper on Earth Orbit Synthesis. Dennett-Thorpe & de Bruyn (2000) define the time-scale by use of the structure function (e.g. Simonetti et al., 1985). Their definition of the variability time-scale corresponds to the full-width at $1/e$ of the ACF, or $2t_{\rm dc}$. Rickett et al. (1995) and Rickett et al. (2002) define the time-scale as the half-width at half maximum of the ACF, which for convenience is henceforth written as $t_{0.5}$, and which is in general slightly smaller than $t_{\rm dc}$.

For extragalactic sources, in addition to the above, several other "counting" parameters have been used in the literature. This is possible because the observed IDV is often quasi-sinusoidal. Kedziora-Chudczer et al. (1997) used the mean peak-to-peak time, while Jauncey & Macquart (2001) used the mean peak-to-trough or trough-to-peak time. While estimates from the ACF or structure function are often more reliable as they do not depend on analysis by eye, "counting" methods remain useful, particularly where the original data are unavailable.

While choosing a definition for the time-scale is a matter of convention, it is necessary to use a consistent method when comparing theoretical and observational results. So far, time-scales have been analysed in detail only for one source, PKS 1257−326, and this analysis is presented in Section 6.4.1. The characteristic time-scale here is defined as the half-width at half-maximum of the autocorrelation function, $t_{0.5}$. ACFs have been calculated using the discrete correlation method and binning into time lag intervals (Edelson & Krolik, 1988), rather than interpolating the data. The discrete correlation method has the advantage that it is straight-forward to combine data from two (or more) consecutive days without interpolating across 12 hour gaps. The mean

is first subtracted from each data point and the ACF is normalised to unity at zero lag. Specifically, the method is as follows. For each pair of data points i, j, the lag $(t_i - t_j)$ and the function $C_{ij} = [(S(t_i) - \bar{S})(S(t_j) - \bar{S})]/\sigma_S^2$ are calculated, where $S(t_i)$ is the flux density at time t_i, $\bar{S}$ is the mean flux density for the particular dataset, and σ_S^2 is the corresponding variance of S for the dataset, minus the variance expected due to errors. The elements C_{ij} are then binned according to lag, and the average C_{ij} is taken as the estimate of the ACF for each bin, provided a significant number of elements lie within that bin.

The largest uncertainties in any estimate of characteristic time-scales are due to the finite sampling of the scintillation pattern, and the uncertainties in our understanding of the underlying stochastic process. Scintillation patterns for AGN are quite often observed to be quasi-sinusoidal, and thus the pattern can be thought of as a "band-limited function", but the exact form of this "function" is not easy to determine from limited sampling of a scintillation pattern. Observations over many "scintels" are required to obtain a reliable estimate of time-scale. In Section 6.4.1, the uncertainties in time-scale estimates have been derived empirically by dividing the data into subsets, for the particular case of PKS 1257−326.

5.6 Overall results

Table 5.3 presents the mean flux densities and rms variations in Stokes I, Q and U, measured for all sources in Table 5.1 between February 2001 and February 2002. Also included at the end of the table are the same values for the calibration sources (listed in Table 2.1. Note that although PKS 1921−293 is listed in Table 2.1 since it was used to derive gain curves, it was actually one of the target sources, although no significant IDV was observed.) The data of 2001 July 26 are not included in the statistics presented in the Table 5.3, due to the rms scatter in calibration source data for this observation being a factor of ~ 3 larger than usual.

Although it is rather complex, Table 5.3 quantifies the variability characteristics of all observed sources. The columns and rows of Table 5.3 are as follows. Column 1 lists the IAU standard source name in B1950 coordinates (except for the two PMN Survey sources, where the J2000 name is used instead; refer to Table 5.1 for the full catalog names). Column 2 indicates the observing frequency in GHz. For each source there are three rows of data at each frequency. Column 3 labels each row, where "Range" gives the minimum and maximum value for each quantity, "Mean" refers to the average of all datasets, and "L-T" indicates long-term variability, from the combined datasets. Columns 4 and 5 list statistics for total flux density. The mean total flux densities, in Jy, are given in column 4. The "Range" of $\langle I \rangle$ thus gives the lowest average and highest average flux density for any given epoch, while the rows labelled "L-T" give the long-term average flux density. Column 5 gives the modulation index for total flux density, μ_I, as a percentage. The "Range" of μ_I is the lowest and highest μ_I observed for any one dataset, while the "Mean" μ_I is the average of the μ_I values for each dataset. The rows labelled "L-T" give the long-term μ_I, from all datasets combined. Columns 6 and

9 list the mean values, in mJy, for Stokes Q and U, respectively, where the rows are the same as for $\langle I \rangle$ in column 4. Columns 7 and 10 list σ_Q and σ_U, respectively, in mJy. Columns 8 and 11 list σ_Q/I and σ_U/I, respectively, as a percentage of the total flux density. The range, mean, and long-term values are defined just as for Stokes I in column 5.

The reason for including both σ_Q and σ_Q/I (and the corresponding quantities for Stokes U) in the table is that both are important for a quick assessment of the level of variability in linear polarization. In general, sources are considered variable in linear polarization only if σ_Q or σ_U is larger than 1 mJy *and* σ_Q/I or σ_U/I is greater than 0.3%. Variability below this level may be significant, however some leakage errors near transit were evident in Stokes Q and U light curves for two strong sources which pass close to the zenith (PKS 1921−293 and PKS 1622−297) and this effect needs to be further investigated before lower level variability in Stokes Q and U can be confirmed.

From the modulation indices in column 5, and also from the rms variations in Stokes Q and U, listed in columns 7 and 10, it can be seen that although some sources do not show significant IDV, all apart from the calibration sources show variability on longer timescales. It is also notable that for those sources which exhibit significant IDV, a large range is observed in the modulation indices from different sessions. Partly this is due to the differing session lengths: statistics from the shorter, 12 hour sessions in August 2001 have been included in the table. Most sources vary on time-scales longer than 12 hours, and modulation indices for these shorter sessions would often be lower than those for the longer sessions. The modulation index also varies from session to session simply due to the stochastic nature of the process and limited sampling. Also, the *annual cycle* effect means that the characteristic time-scale changes over the course of a year; some sources may have characteristic time-scales much longer than 48 hours at certain times of the year, and hence in some sessions no significant variability would be osberved. Finally, if intrinsic changes in the source or changes in the average "screen" properties occur on a time-scale of several months, these could lead to a change in μ.

One of the aims of ATCA project C927 was to investigate if there is any connection between IDV and large fractional circular polarization (CP), given the strong and variable CP found for PKS 1519−273 (Macquart et al., 2000). So far, circular polarization data have only been analysed for the first three observing sessions in 2001, at 4.8 GHz. IDV in circular polarization has not yet been examined in detail, except for PKS 1519−273, the results for which are to be presented elsewhere (Johnston et al., in preparation). Average Stokes V measurements for all sources observed in the first three epochs are presented in Table 5.4. Both the V flux density (measured from an image) and fractional circular polarization, V/I are shown. Both these numbers have been "zero-point" corrected, following the assumption that the primary calibrator PKS 1934−638 has no circular polarization. Careful measurements by Rayner et al. (2000) showed PKS 1934−638 to have a small amount of circular polarization, and this has been corrected for as outlined by (Rayner, 2001) in the ATCA Circular Polarization Users Guide.

Table 5.3: ATCA project C927 results. Modulation indices for IDV and long-term variability in Stokes I, Q and U. See Section 5.6 for explanation of columns and rows.

(1)	(2)	(3)	(4)	(5)	(6)	(7)	(8)	(9)	(10)	(11)
Source	ν GHz		$\langle I \rangle$ (Jy)	μ_I (%)	$\langle Q \rangle$ (mJy)	σ_Q (mJy)	σ_Q/I (%)	$\langle U \rangle$ (mJy)	σ_U (mJy)	σ_U/I (%)
0104−408	4.8	Range	2.22, 3.09	0.3, 1.7	−68.7, −10.8	2.5, 5.2	0.11, 0.17	−17.7, 49.0	2.3, 5.4	0.09, 0.18
		Mean		0.9		3.6	0.13		3.5	0.13
		L-T	2.77	11.2	−42.8	20.5	0.74	18.4	24.6	0.89
	8.6	Range	2.58, 3.71	0.4, 0.8	−167, −7.0	2.7, 4.7	0.08, 0.15	−96.7, 14.6	2.0, 5.4	0.07, 0.15
		Mean		0.5		3.6	0.11		4.2	0.12
		L-T	3.42	11.8	−82.2	70.5	2.06	−18.4	33.7	0.98
0235+164	4.8	Range	1.23, 1.64	0.5, 1.9	−7.5, 21.6	0.6, 5.0	0.04, 0.33	−5.8, 6.8	0.1, 3.8	0.00, 0.24
		Mean		1.3		2.3	0.16		1.9	0.13
		L-T	1.40	8.7	7.1	7.7	0.55	−0.4	3.9	0.28
	8.6	Range	1.37, 1.74	0.4, 1.3	−21.9, 39.1	1.4, 3.3	0.09, 0.20	−11.0, 19.8	1.4, 3.4	0.08, 0.22
		Mean		1.0		2.3	0.15		2.2	0.14
		L-T	1.57	7.3	13.6	19.7	1.26	4.5	9.3	0.60
0346−279	4.8	Range	1.01, 1.37	0.5, 1.8	11.3, 25.2	0.7, 2.3	0.06, 0.17	6.0, 28.0	1.8, 3.9	0.16, 0.29
		Mean		1.1		1.3	0.11		2.3	0.19
		L-T	1.18	10.9	18.7	4.1	0.35	18.6	8.5	0.72
	8.6	Range	1.03, 1.65	0.2, 1.1	−1.1, 18.5	0.9, 1.6	0.08, 0.12	−12.4, 23.5	0.2, 3.3	0.02, 0.24
		Mean		0.7		1.3	0.10		1.6	0.12
		L-T	1.35	13.8	11.6	6.6	0.49	9.7	13.4	1.00
0405−385	4.8	Range	0.78, 1.00	0.2, 1.6	5.7, 14.0	0.4, 2.4	0.04, 0.25	−7.0, 3.1	0.5, 1.3	0.06, 0.14
		Mean		0.7		0.9	0.10		1.0	0.11
		L-T	0.86	9.2	9.1	3.2	0.38	−3.8	3.9	0.46
	8.6	Range	0.87, 1.23	0.3, 0.9	−0.1, 16.6	0.5, 2.0	0.04, 0.17	−9.8, 10.9	0.8, 1.7	0.07, 0.15
		Mean		0.6		1.1	0.10		1.2	0.11
		L-T	1.04	12.9	8.1	4.2	0.41	−3.4	6.8	0.66

(1)	(2)	(3)	(4)	(5)	(6)	(7)	(8)	(9)	(10)	(11)
Source	ν		$\langle I\rangle$ (Jy)	μ_I (%)	$\langle Q\rangle$ (mJy)	σ_Q (mJy)	σ_Q/I (%)	$\langle U\rangle$ (mJy)	σ_U (mJy)	σ_U/I (%)
0502+049	4.8	Range	0.75, 0.85	0.3, 2.1	12.5, 17.5	0.9, 1.2	0.10, 0.16	−31.2, −24.1	0.9, 1.4	0.12, 0.17
		Mean		1.2		1.0	0.13		1.1	0.14
		L-T	0.81	5.0	15.2	2.1	0.26	−29.5	2.9	0.36
	8.6	Range	0.74, 0.81	0.5, 1.7	3.4, 11.0	1.0, 1.4	0.13, 0.19	−37.1, −25.7	1.1, 1.6	0.14, 0.22
		Mean		1.0		1.2	0.16		1.4	0.18
		L-T	0.78	3.5	7.7	3.5	0.45	−29.0	5.2	0.66
0506+056	4.8	Range	0.51, 0.67	2.1, 4.3	−7.8, 11.2	0.9, 2.7	0.14, 0.41	−11.9, 2.5	0.7, 2.5	0.11, 0.38
		Mean		3.0		1.6	0.26		1.4	0.23
		L-T	0.62	9.8	−0.9	8.2	1.32	−8.7	5.2	0.83
	8.6	Range	0.52, 0.66	1.6, 5.5	−6.3, 0.9	0.8, 3.7	0.13, 0.56	−16.9, −7.0	2.0, 2.7	0.32, 0.47
		Mean		3.1		2.1	0.35		2.2	0.38
		L-T	0.61	9.5	−2.7	3.7	0.61	−9.4	4.4	0.72
0524+034	4.8	Range	0.33, 0.41	0.5, 1.7	0.6, 3.8	0.5, 0.9	0.14, 0.22	−5.0, 0.9	0.4, 0.9	0.10, 0.26
		Mean		0.9		0.7	0.17		0.6	0.16
		L-T	0.38	8.6	2.6	1.6	0.42	−2.3	2.5	0.66
	8.6	Range	0.40, 0.43	2.3, 4.1	4.1, 5.9	0.9, 1.0	0.22, 0.23	−7.7, −3.5	1.0, 1.0	0.25, 0.26
		Mean		3.1		0.9	0.23		1.0	0.25
		L-T	0.42	4.3	4.9	1.3	0.31	−5.5	2.4	0.58
0537−441	4.8	Range	4.66, 7.11	0.1, 1.4	140, 321	1.5, 10.1	0.03, 0.21	−93.6, −12.2	2.3, 8.7	0.04, 0.18
		Mean		0.7		5.2	0.09		5.1	0.09
		L-T	5.69	10.4	211	57.7	1.02	−46.3	23.3	0.41
	8.6	Range	4.57, 8.00	0.2, 2.0	79.7, 454	5.0, 17.4	0.09, 0.23	−186, −100	5.1, 12.1	0.07, 0.22
		Mean		0.8		8.9	0.14		7.8	0.13
		L-T	6.22	12.5	214	107	1.71	−120	26.4	0.42
1034−293	4.8	Range	0.95, 1.50	1.0, 5.8	−38.4, −5.3	1.2, 4.0	0.12, 0.30	−22.0, 11.1	2.0, 5.3	0.17, 0.49
		Mean		2.7		2.3	0.19		3.4	0.29
		L-T	1.15	13.9	−16.0	10.7	0.92	−5.4	10.6	0.92
	8.6	Range	1.19, 1.72	0.6, 7.1	−84.4, −44.6	2.0, 8.9	0.13, 0.66	−68.3, −30.7	1.8, 6.0	0.14, 0.47
		Mean		3.5		5.3	0.39		3.5	0.26
		L-T	1.35	11.5	−56.3	14.8	1.10	−42.7	11.4	0.85

(1)	(2)	(3)	(4)	(5)	(6)	(7)	(8)	(9)	(10)	(11)
Source	ν		$\langle I\rangle$ (Jy)	μ_I (%)	$\langle Q\rangle$ (mJy)	σ_Q (mJy)	σ_Q/I (%)	$\langle U\rangle$ (mJy)	σ_U (mJy)	σ_U/I (%)
J1047−6217	4.8	Range	0.63, 0.98	0.6, 2.2	−39.4, −19.9	0.7, 1.2	0.09, 0.15	−6.2, 11.1	0.7, 1.1	0.08, 0.14
		Mean		1.4		0.9	0.11		0.9	0.11
		L-T	0.83	13.2	−27.8	6.5	0.79	1.8	5.8	0.70
	8.6	Range	0.90, 1.23	0.9, 6.0	−32.1, 4.7	0.9, 3.8	0.09, 0.31	−5.2, 44.2	0.7, 4.1	0.07, 0.38
		Mean		3.4		1.8	0.16		2.1	0.19
		L-T	1.08	7.8	−13.8	10.3	0.95	20.5	17.9	1.65
1144−379	4.8	Range	1.32, 2.36	1.2, 9.6	−81.1, −2.3	3.4, 7.7	0.18, 0.35	−38.1, 42.6	4.1, 17.2	0.30, 0.90
		Mean		4.7		5.0	0.28		10.2	0.58
		L-T	1.85	18.9	−37.9	25.3	1.37	3.6	32.7	1.77
	8.6	Range	1.66, 3.06	1.0, 7.3	−129, −10.2	9.1, 25.7	0.34, 0.84	−5.3, 53.5	7.1, 35.2	0.34, 1.15
		Mean		3.9		13.3	0.57		17.6	0.73
		L-T	2.38	19.4	−58.9	41.3	1.73	33.7	30.3	1.27
1257−326	4.8	Range	0.20, 0.24	5.1, 9.2	−0.4, 0.8	0.5, 0.9	0.21, 0.44	5.8, 7.3	0.5, 0.8	0.23, 0.40
		Mean		7.7		0.6	0.30		0.6	0.30
		L-T	0.22	11.1	0.1	0.7	0.32	6.4	0.8	0.35
	8.6	Range	0.21, 0.30	3.3, 5.8	−6.3, 1.9	0.4, 1.0	0.16, 0.44	2.3, 5.1	0.5, 1.8	0.20, 0.61
		Mean		5.0		0.7	0.30		0.9	0.34
		L-T	0.26	14.2	−2.4	3.2	1.24	3.9	1.5	0.56
J1326−5256	4.8	Range	1.16, 1.89	1.3, 15.7	−20.0, 56.9	1.1, 8.6	0.06, 0.70	−40.7, 7.1	1.2, 7.4	0.10, 0.61
		Mean		6.3		4.1	0.28		3.4	0.23
		L-T	1.52	19.2	13.6	25.3	1.67	−16.6	17.8	1.17
	8.6	Range	1.65, 2.70	0.7, 15.8	−50.0, 70.8	2.6, 13.1	0.10, 0.69	−91.9, 16.4	3.5, 12.4	0.14, 0.64
		Mean		6.6		7.7	0.38		7.8	0.38
		L-T	2.11	17.1	5.0	41.0	1.94	−28.6	33.6	1.59
1415−349	4.8	Range	0.47, 0.51	0.8, 3.3	20.8, 23.5	0.7, 1.3	0.13, 0.27	−10.9, −8.2	0.7, 1.8	0.15, 0.38
		Mean		1.8		1.0	0.21		1.2	0.25
		L-T	0.48	3.2	21.7	1.3	0.26	−9.2	1.5	0.30
	8.6	Range	0.38, 0.43	1.1, 3.9	16.9, 22.1	0.4, 1.2	0.11, 0.31	−3.3, −2.0	0.8, 1.5	0.20, 0.36
		Mean		1.8		0.9	0.24		1.1	0.26
		L-T	0.40	3.5	20.1	1.9	0.49	−2.6	1.2	0.29

(1)	(2)	(3)	(4)	(5)	(6)	(7)	(8)	(9)	(10)	(11)
Source	ν		$\langle I \rangle$ (Jy)	μ_I (%)	$\langle Q \rangle$ (mJy)	σ_Q (mJy)	σ_Q/I (%)	$\langle U \rangle$ (mJy)	σ_U (mJy)	σ_U/I (%)
1519−279	4.8	Range	1.70, 2.06	2.0, 11.2	−16.4, 52.3	6.4, 25.8	0.34, 1.27	−57.5, 16.1	8.6, 20.5	0.44, 1.12
		Mean		4.5		13.9	0.74		14.5	0.79
		L-T	1.82	8.3	21.0	25.8	1.41	−14.0	28.7	1.57
	8.6	Range	1.89, 2.09	2.3, 5.6	23.9, 68.9	7.0, 27.3	0.37, 1.38	−35.9, 48.1	11.3, 26.2	0.56, 1.27
		Mean		3.5		18.5	0.91		17.9	0.88
		L-T	2.01	5.0	44.1	24.4	1.21	3.1	30.3	1.51
1622−253	4.8	Range	1.09, 2.51	1.9, 11.1	−23.1, 3.3	1.4, 9.9	0.12, 0.47	−7.0, 21.9	2.4, 7.6	0.13, 0.47
		Mean		5.7		4.4	0.22		4.4	0.24
		L-T	1.74	29.7	−7.9	9.9	0.57	9.1	10.2	0.59
	8.6	Range	1.33, 3.22	1.0, 10.8	−28.4, 23.7	3.5, 11.1	0.19, 0.40	−22.5, 55.0	3.5, 14.1	0.12, 0.56
		Mean		4.7		7.5	0.30		8.0	0.32
		L-T	2.36	29.3	2.2	16.7	0.71	18.1	22.8	0.97
1622−297	4.8	Range	2.43, 3.02	0.5, 3.7	103, 185	2.1, 5.2	0.07, 0.21	19.3, 73.9	4.6, 11.1	0.16, 0.41
		Mean		1.4		3.2	0.12		6.8	0.25
		L-T	2.76	6.4	140	21.7	0.79	44.5	15.5	0.56
	8.6	Range	2.13, 2.76	0.7, 3.8	105, 137	3.3, 11.2	0.13, 0.51	91.9, 123	4.4, 13.7	0.20, 0.55
		Mean		1.9		6.2	0.26		7.5	0.30
		L-T	2.52	9.3	125	11.9	0.47	105	11.0	0.44
1921−293	4.8	Range	11.22, 12.30	0.2, 0.8	−146, 421	4.3, 13.0	0.04, 0.11	−137, 148	5.9, 26.8	0.05, 0.23
		Mean		0.5		8.1	0.07		13.4	0.11
		L-T	11.68	2.9	201	205	1.76	−11.4	91.2	0.78
	8.6	Range	13.06, 14.41	0.2, 0.9	−201, 718	8.6, 14.8	0.06, 0.11	−258, 101	14.5, 39.5	0.11, 0.29
		Mean		0.5		11.0	0.08		23.6	0.17
		L-T	13.67	2.6	329	331	2.42	−42.6	122	0.89
1958−179	4.8	Range	1.53, 2.19	0.3, 1.3	−1.7, 40.2	1.1, 4.2	0.06, 0.25	−9.9, 58.0	0.7, 4.1	0.03, 0.19
		Mean		0.7		2.4	0.13		1.9	0.10
		L-T	1.76	11.5	13.5	12.8	0.73	19.5	18.5	1.05
	8.6	Range	1.67, 2.53	0.3, 1.2	−29.4, 33.1	1.3, 4.9	0.07, 0.30	7.5, 61.4	1.5, 4.1	0.07, 0.23
		Mean		0.6		3.4	0.18		3.1	0.17
		L-T	1.93	13.6	−0.7	19.5	1.01	21.5	15.8	0.82

(1)	(2)	(3)	(4)	(5)	(6)	(7)	(8)	(9)	(10)	(11)
Source	ν		$\langle I \rangle$ (Jy)	μ_I (%)	$\langle Q \rangle$ (mJy)	σ_Q (mJy)	σ_Q/I (%)	$\langle U \rangle$ (mJy)	σ_U (mJy)	σ_U/I (%)
2155−304	4.8	Range	0.28, 0.39	0.7, 1.8	5.8, 11.5	0.4, 1.5	0.13, 0.39	−13.1, −7.1	0.3, 1.4	0.11, 0.36
		Mean		1.3		1.0	0.29		1.0	0.28
		L-T	0.35	9.7	9.1	2.1	0.59	−9.7	2.6	0.75
	8.6	Range	0.28, 0.39	0.6, 1.3	2.6, 10.8	0.7, 1.7	0.23, 0.48	−12.2, −4.8	0.5, 1.1	0.15, 0.37
		Mean		0.9		1.2	0.35		0.9	0.26
		L-T	0.35	10.2	7.5	3.4	0.97	−8.9	2.9	0.84
2201+171	4.8	Range	0.53, 0.97	1.5, 3.2	−6.3, 21.9	1.1, 3.2	0.19, 0.44	−25.7, −12.4	0.7, 3.4	0.13, 0.37
		Mean		2.1		2.4	0.33		1.7	0.23
		L-T	0.64	25.2	2.2	9.6	1.49	−23.5	5.0	0.78
	8.6	Range	0.53, 1.15	0.9, 3.5	−7.3, 1.3	0.8, 2.0	0.15, 0.18	−25.6, 0.6	1.1, 1.7	0.15, 0.20
		Mean		2.2		1.4	0.16		1.4	0.18
		L-T	0.72	32.7	−4.2	4.0	0.55	−16.9	10.9	1.53
0237−233	4.8	Range	2.73, 2.81	0.1, 0.4	10.9, 14.9	0.1, 1.9	0.01, 0.07	−87.9, −86.7	0.2, 1.5	0.01, 0.06
		Mean		0.2		1.3	0.04		1.0	0.04
		L-T	2.78	0.6	13.3	2.0	0.07	−87.4	1.1	0.04
	8.6	Range	1.59, 1.67	0.1, 0.7	14.9, 18.2	0.4, 1.8	0.03, 0.11	−51.8, −43.7	0.6, 1.6	0.03, 0.10
		Mean		0.4		1.1	0.07		1.2	0.07
		L-T	1.64	1.0	16.5	1.5	0.09	−48.6	3.1	0.19
0823−500	4.8	Range	3.00, 3.22	0.1, 0.3	−51.2, −44.7	0.4, 1.4	0.01, 0.05	3.2, 5.3	0.6, 2.1	0.02, 0.07
		Mean		0.2		0.9	0.03		1.2	0.04
		L-T	3.07	2.1	−48.6	2.2	0.07	4.5	1.4	0.05
	8.6	Range	1.44, 1.53	0.2, 0.7	20.3, 24.5	0.5, 1.4	0.04, 0.10	0.3, 2.0	0.8, 1.6	0.05, 0.11
		Mean		0.4		0.9	0.06		1.2	0.08
		L-T	1.49	1.7	22.8	1.3	0.09	1.2	1.2	0.08
1127−145	4.8	Range	4.13, 4.27	0.1, 0.3	85.9, 104	1.4, 2.9	0.03, 0.07	−105, −63.9	1.2, 2.6	0.03, 0.06
		Mean		0.2		1.9	0.05		1.8	0.04
		L-T	4.21	0.7	97.0	6.5	0.15	−91.9	12.0	0.28
	8.6	Range	3.41, 3.56	0.2, 0.6	32.5, 73.3	1.0, 3.7	0.03, 0.11	−117, −84.6	2.1, 3.8	0.06, 0.11
		Mean		0.3		2.2	0.06		2.7	0.08
		L-T	3.49	1.1	56.8	12.7	0.36	−103	10.3	0.29

(1)	(2)	(3)	(4)	(5)	(6)	(7)	(8)	(9)	(10)	(11)
Source	ν		$\langle I \rangle$ (Jy)	μ_I (%)	$\langle Q \rangle$ (mJy)	σ_Q (mJy)	σ_Q/I (%)	$\langle U \rangle$ (mJy)	σ_U (mJy)	σ_U/I (%)
1934−638	4.8	Range	5.70, 5.83	0.1, 0.3	−1.1, 0.5	1.1, 2.3	0.02, 0.04	−1.2, 1.0	0.8, 4.3	0.01, 0.07
		Mean		0.2		1.6	0.03		2.3	0.04
		L-T	5.82	0.5	−0.1	1.7	0.03	0.0	2.6	0.04
	8.6	Range	2.73, 2.85	0.2, 0.6	−1.2, 0.6	1.0, 2.7	0.03, 0.10	−0.4, 0.4	0.7, 2.8	0.02, 0.10
		Mean		0.4		1.6	0.06		1.7	0.06
		L-T	2.84	0.9	0.0	1.7	0.06	−0.1	1.8	0.06
2126−158	4.8	Range	1.21, 1.26	0.1, 0.3	−0.9, 0.2	0.4, 1.2	0.04, 0.10	0.8, 2.0	0.5, 1.1	0.04, 0.09
		Mean		0.2		0.8	0.06		0.8	0.07
		L-T	1.23	1.5	−0.3	0.8	0.07	1.2	0.9	0.08
	8.6	Range	1.14, 1.21	0.2, 0.4	−1.5, −0.4	0.5, 1.1	0.05, 0.09	−0.7, 0.3	0.4, 1.4	0.03, 0.12
		Mean		0.3		0.9	0.07		0.9	0.07
		L-T	1.18	1.1	−0.9	0.9	0.08	−0.2	0.9	0.08
2134+004	4.8	Range	10.00, 10.27	0.1, 0.3	−111.4, −68.8	1.3, 7.1	0.01, 0.07	−57.0, −42.2	2.0, 6.0	0.02, 0.06
		Mean		0.2		4.2	0.04		3.7	0.04
		L-T	10.18	1.0	−81.0	16.1	0.16	−51.7	6.6	0.06
	8.6	Range	8.41, 9.00	0.1, 0.7	−1.1, 31.9	1.6, 8.3	0.02, 0.09	150.8, 190.5	2.3, 9.0	0.03, 0.10
		Mean		0.3		5.5	0.06		5.0	0.06
		L-T	8.81	1.9	10.9	14.6	0.17	165	16.0	0.18

Also shown in Table 5.4 is the mean spectral index of each source, and the mean linear polarization over all observing sessions. The final column of Table 5.4 lists "variability flags" for the source, based on the data shown in Table 5.3. 'I' indicates that the source showed significant IDV in Stokes I in at least one session, while 'p' indicates that significant IDV in linearly polarized flux density was observed. 'L' indicates that only longer-term variability was observed. 'C' indicates calibration sources. PKS 0823−500, a calibration source often used at the ATCA, is a long-term variable and therefore is not a high-quality flux density calibrator.

The most strongly circularly polarized extragalactic source yet found is the high-redshift ($z = 3.27$) GPS source PKS 2126−158, one of the calibration sources which does not show any short-term variability. There is no straightforward correlation, therefore, between IDV and high fractional circular polarization. However, IDV sources may show much more *variable* circular polarization, and this will be further investigated elsewhere. Only one source, PMN J1326−5256, showed a sign change in the average V flux density between sessions. This sign change could occur due to oppositely circularly polarized components in the source, at least one of which scintillates. PMN J1326−5256 was one of the strongest IDV sources observed in the present program.

5.7 Selected results for individual sources

This section briefly discusses the behaviour of some of the stronger IDV sources. For each source, an example of the IDV observed in Stokes I, Q and U is shown. Also, the combined data from all epochs are shown in a single plot. From this it is possible to see the amplitude of variability in all epochs, as well as any overall long-term trends. The combined plot does not indicate the time-scale of the variability seen within each epoch. So far, changes in characteristic time-scale have been analysed in detail for only one source, PKS 1257−326, which showed by far the most rapid variability of any source observed. The results for PKS 1257−326 are presented in Chapter 6. More detailed analysis of the other sources is a longer-term project and will be presented in subsequent publications.

5.7.1 PMN J1047−6217

The low Galactic latitude ($b_{II} = -2.8°$) of PMN J1047−6217 means it is likely to have a high transition frequency between weak and strong scattering (Walker, 1998). Indeed this source showed much larger amplitude IDV at 8.6 GHz than at 4.8 GHz, as expected if the transition frequency is closer to 8.6 GHz than to 4.8 GHz. The average modulation index for total flux density in each session at 8.6 GHz was $\langle \mu_I \rangle = 3.4\%$, compared with $\langle \mu_I \rangle = 1.4\%$ at 4.8 GHz. The modulation index for long-term variability, however, was larger at 4.8 GHz. This observed behaviour is consistent with 4.8 GHz being in the regime of strong scattering, where refractive scintillation time-scales are significantly longer than in weak scattering. The other IDV sources are at higher Galactic latitudes, and all show either similar modulation indices at 4.8 and 8.6 GHz,

Table 5.4: Average parameters and variability flags for sources observed in the ATCA C927 program. $\langle\alpha_{4.8}^{8.6}\rangle$ is the mean spectral index between 4.8 and 8.6 GHz. $\langle V_{4.8}\rangle$ is the mean circularly polarized flux density in mJy at 4.8 GHz, from three observing sessions only. $\langle V/I\rangle$ is the mean percentage circular polarization. Both $\langle V_{4.8}\rangle$ and $\langle V/I\rangle$ have been "zero-point corrected" assuming PKS 1934−638 has $V/I = 0.03\%$, following Rayner (2001). Also shown for comparison is the mean percentage linear polarization at 4.8 GHz, $\langle p_{4.8}/I\rangle$. The letters shown in the final column are as follows: L = long-term variable, but no significant IDV observed. p = Significant IDV observed in Stokes Q and/or U in at least one session. I = significant IDV observed in total flux density. C = calibration source.

Source	$\langle\alpha_{4.8}^{8.6}\rangle$	$\langle V_{4.8}\rangle$ mJy	$\langle V/I\rangle$ %	$\langle p_{4.8}/I\rangle$ %	Flag
PKS 0104−408	0.36	10	0.33	2.0	L
AO 0235+164	0.18	-1.4	−0.11	0.7	p
PKS 0346−279	0.22	-3.5	−0.32	2.3	L
PKS 0405−385	0.33	1.1	0.14	1.3	L
PKS 0502+049	−0.05	< 0.7	<0.09	4.1	I
0506+056	−0.04	< 0.2	<0.03	2.1	Ip
PKS 0524+034	0.14	-	-	1.0	I
PKS 0537−441	0.15	1.1	−0.02	3.8	L
PKS 1034−293	0.27	-0.5	−0.04	1.8	Ip
PMN J1047−6217	0.46	5.8	0.69	3.4	Ip
PKS 1144−379	0.43	5.6	0.27	2.8	Ip
PKS 1257−326	0.28	< 0.2	<0.1	2.9	Ip
PMN J1326−5256[a]	0.64	0.7	0.05	1.8	Ip
PKS 1415−349	−0.33	< 0.3	< 0.06	4.9	Ip
PKS 1519−273	0.17	−18	−0.99	2.3	Ip
PKS 1622−253	0.52	−0.7	−0.05	0.9	Ip
PKS 1622−297	−0.15	−4.8	−0.16	5.3	Ip
PKS 1921−293	0.27	−34	−0.30	2.3	L
PKS 1958−179	0.16	−0.7	−0.04	1.8	L
PKS 2155−304	−0.02	-	-	3.8	p
PKS 2201+171	0.19	< 0.5	< 0.09	3.94	Ip
PKS 0237−233	−0.90	2.3	0.08	3.2	C
PKS 0823−500	−1.23	−3.6	−0.12	1.6	CL
PKS 1127−145	−0.32	−2.0	−0.05	3.2	C
PKS 1934−638[b]	−1.22	0.18	−0.03	0.0	C
PKS 2126−158	−0.06	−17	−1.39	0.1	C
PKS 2134+004	−0.24	6.2	0.06	1.0	C

[a]Sign flip observed for Stokes V between Feb and March 2001. V/I changed from −0.06% to +0.16%.

[b]Primary calibrator. Assumed to have p/I=0, following measurement by Komesaroff et al. (1984). Measured by Rayner et al. (2000) to have $V/I = -0.03\%$.

or else show somewhat larger modulation at 4.8 GHz.

At 8.6 GHz the observed IDV in PMN J1047−6217 was typically 15% peak-to-peak, as shown in the lower panel of Figure 5.4 for the data of 2001 June 2. In contrast, no significant variability was observed over the same two days at 4.8 GHz (upper panel of Figure 5.4), suggesting a characteristic time-scale much longer than two days at this frequency. At 8.6 GHz, the IDV in linearly polarized flux density is observed to be always strongly correlated with the IDV in total intensity, which suggests that the polarized and unpolarized scintillating components of PMN J1047−6217 are coincident and approximately the same size, unlike, for example, the case of PKS 0405−385, which could only be modelled as several scintillating components having different polarizations (Rickett et al., 2002). It is clear that observations over at least two days are required to characterise the short-term variability at 8.6 GHz in PMN J1047−6217. Archival ATCA data on this source, extending back almost 10 years, have been examined, but each dataset extends only over 12 hours, and no IDV larger than a few percent peak-to-peak was observed in the earlier data.

Figure 5.5 shows the combined data from all epochs for PMN J1047−6217. At 4.8 GHz the source shows variations on longer time-scales than sampled by the two-day observing sessions, consistent with this frequency being in the strong scattering regime. The short-term variability at 8.6 GHz is better sampled. There may be a long-term decrease in the intrinsic polarized flux density at 8.6 GHz, between June 2001 (Day 153) and January 2002 (Day 370).

5.7.2 PKS 1144−379

PKS 1144−379 was one of the strongest IDV sources found in the ATCA IDV Survey (Kedziora-Chudczer et al., 2001b), and was also observed in the blazar monitoring program presented in Chapters 3 and 4. All available data on this source indicate that it has a long-lived scintillating component, although the long-term changes suggest that intrinsic variability is also important. The typical "peak-to-trough" time-scale of the short-term variability is on the order of a day. Figure 5.6 shows the data from 2001 Mar 17–19, and from 2001 April 6–7, at 8.6 GHz, for Stokes I, Q and U. The polarized flux density in this source often shows somewhat different behaviour from the total intensity, indicating polarized substructure in the scintillating component, i.e. the source may consist of several components having different fractional linear polarizations and position angles. A superposition of scintillating polarized components can produce variations in linear polarization which are not seen in the total flux density. The data from 2001 March are a good illustration of how the fractional variability in linear polarization can be very large, even though the fractional variability in total flux density is small.

Figure 5.7 shows that while there may be changes in the long-term average Stokes I, Q and U for PKS 1144−379, scintillation is a large contributor to the changes observed in this source.

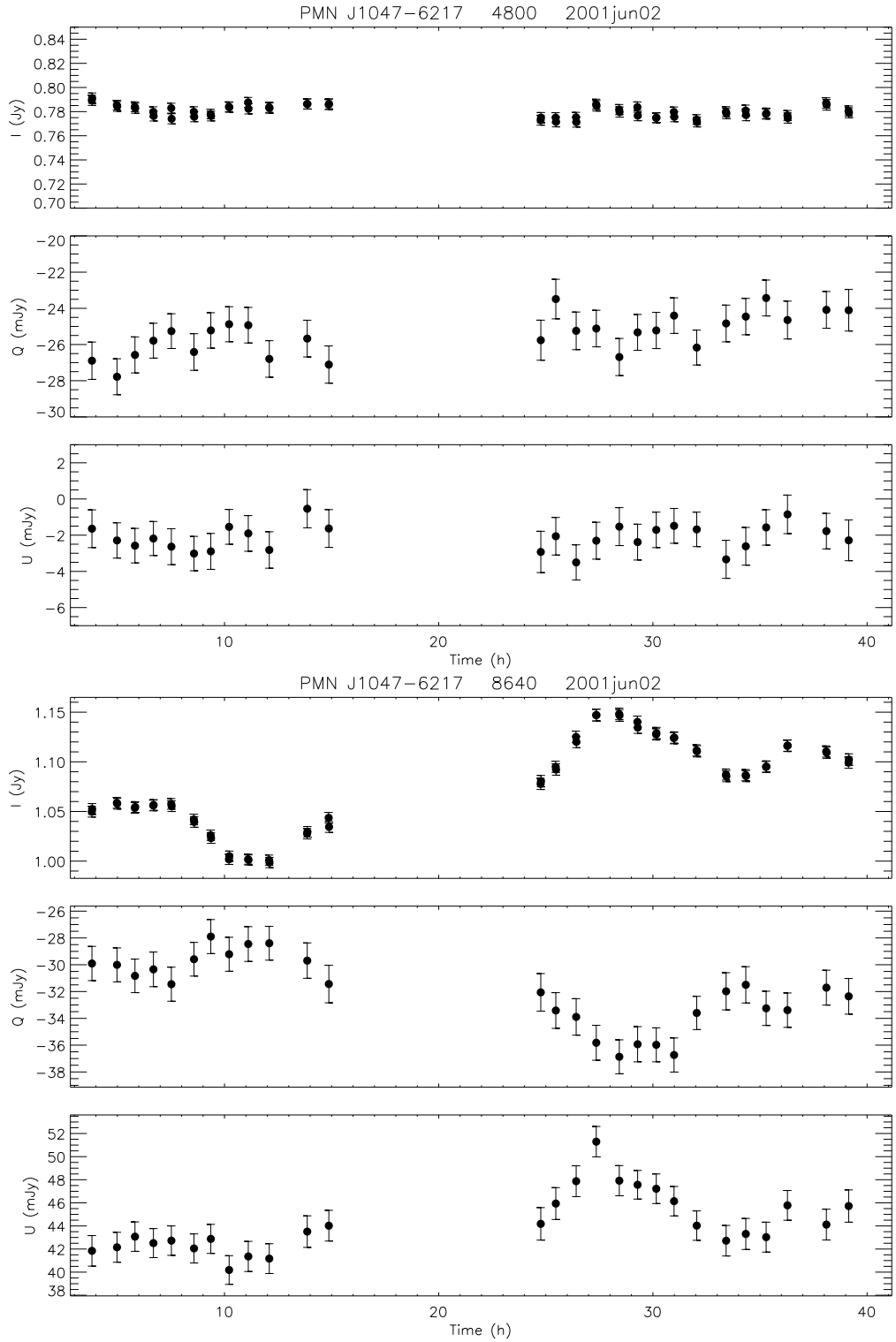

Figure 5.4: PMN J1047−6217: Stokes I, Q and U data at 4.8 GHz (upper panel) and 8.6 GHz (lower panel) from the observation starting on 2001 June 2.

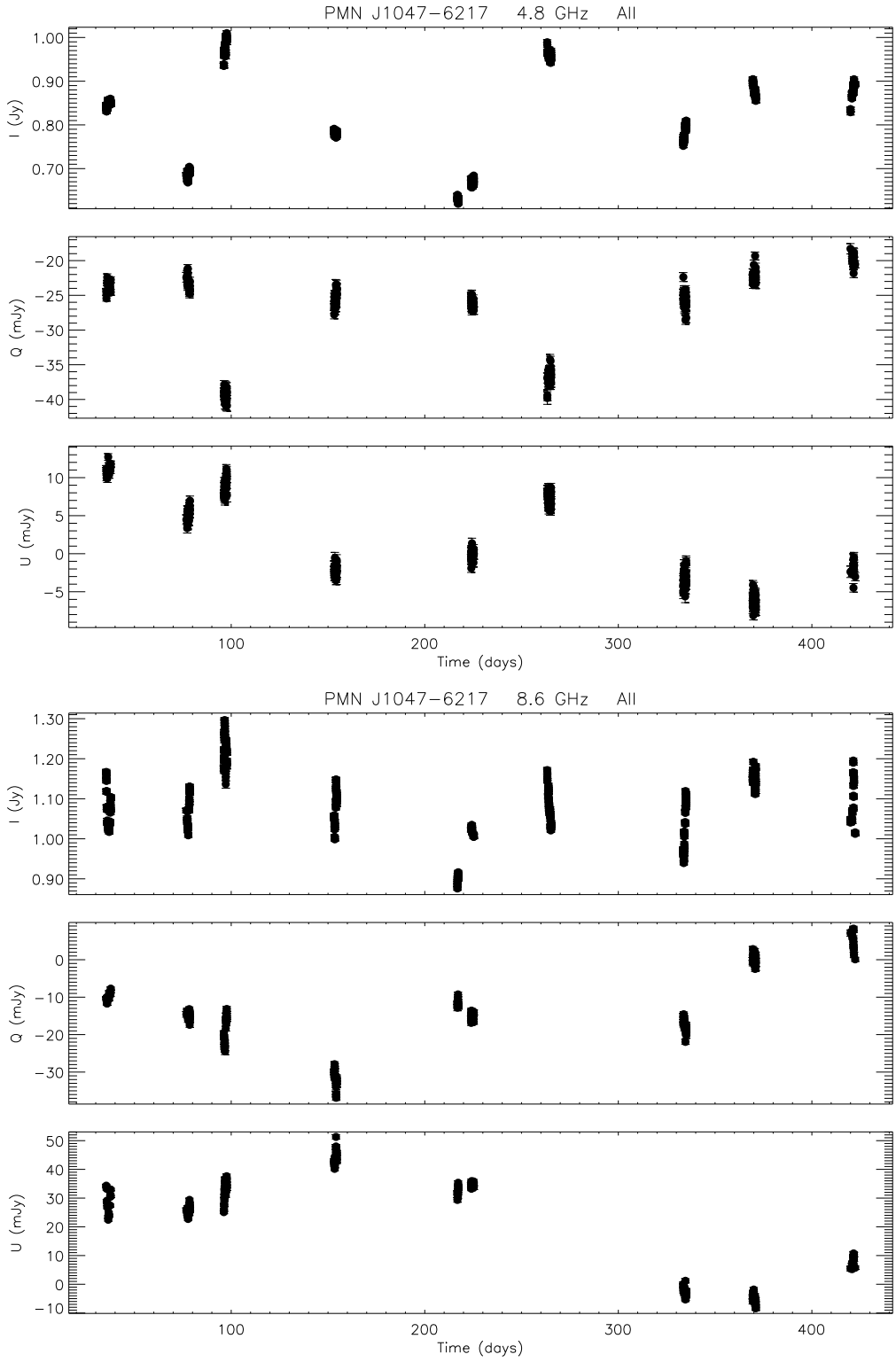

Figure 5.5: PMN J1047−6217: Stokes I, Q and U data at 4.8 and 8.6 GHz from all epochs. Day 0 in this plot is Jan 1, 2001. The data shown in Figure 5.4 start on day 153.

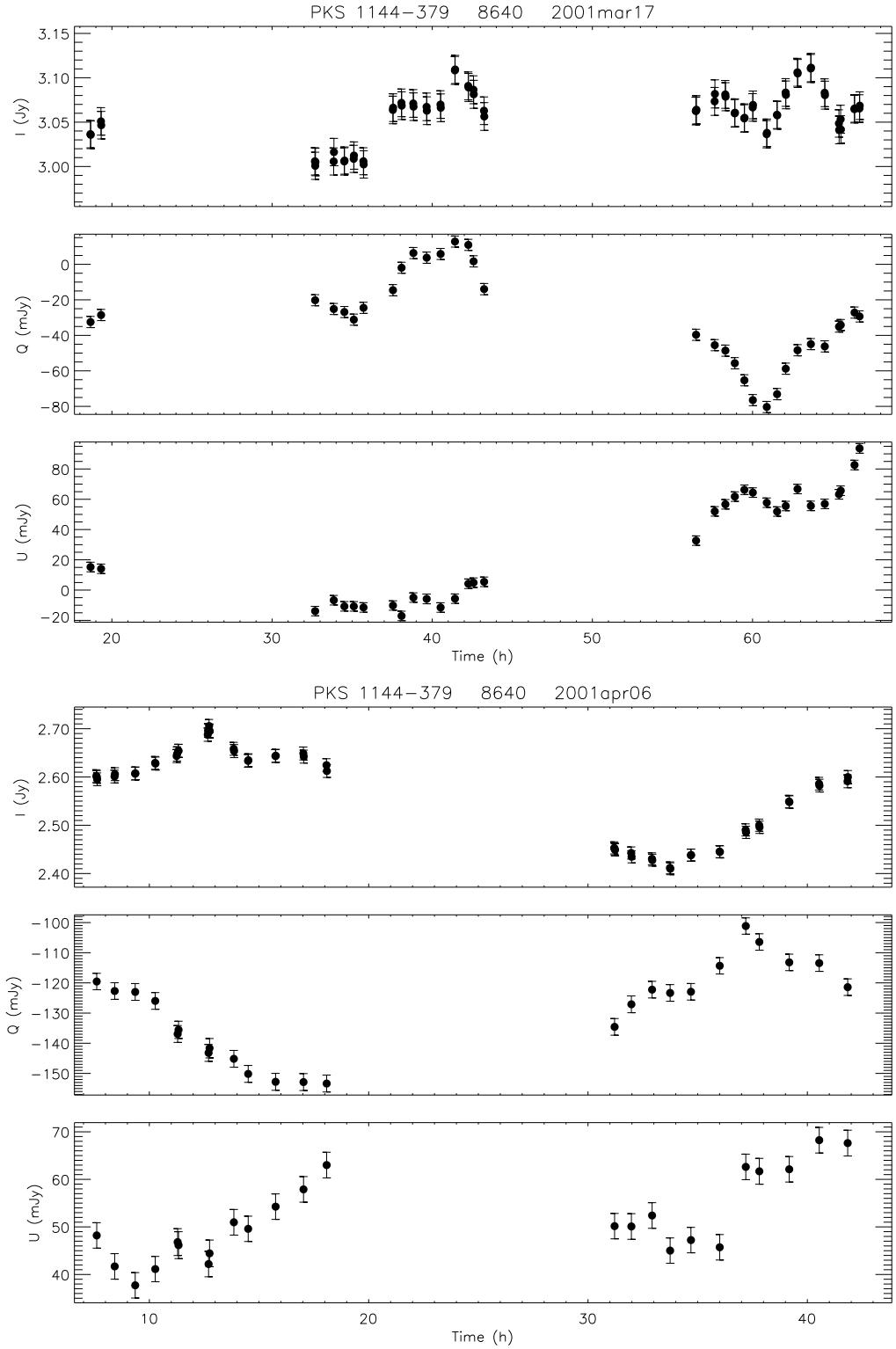

Figure 5.6: PKS 1144−379: Stokes I, Q and U data at 8.6 GHz from the observations starting on 2001 March 17 (upper panel) and 2001 April 6 (lower panel).

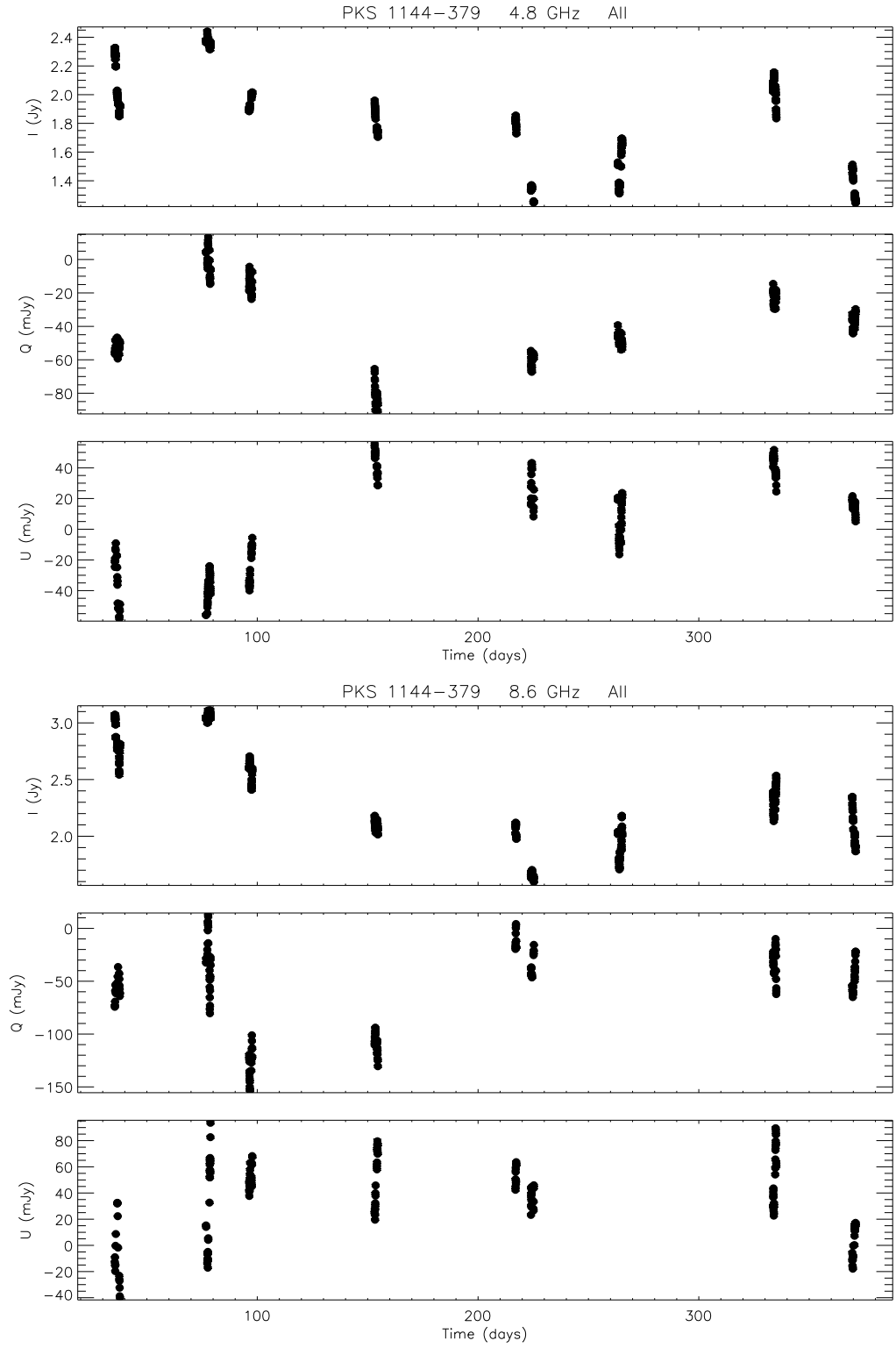

Figure 5.7: PKS 1144−379: Stokes I, Q and U data at 4.8 and 8.6 GHz from all epochs. Day 0 in this plot is Jan 1, 2001. The data shown in Figure 5.6 start on day 76 and day 96, respectively.

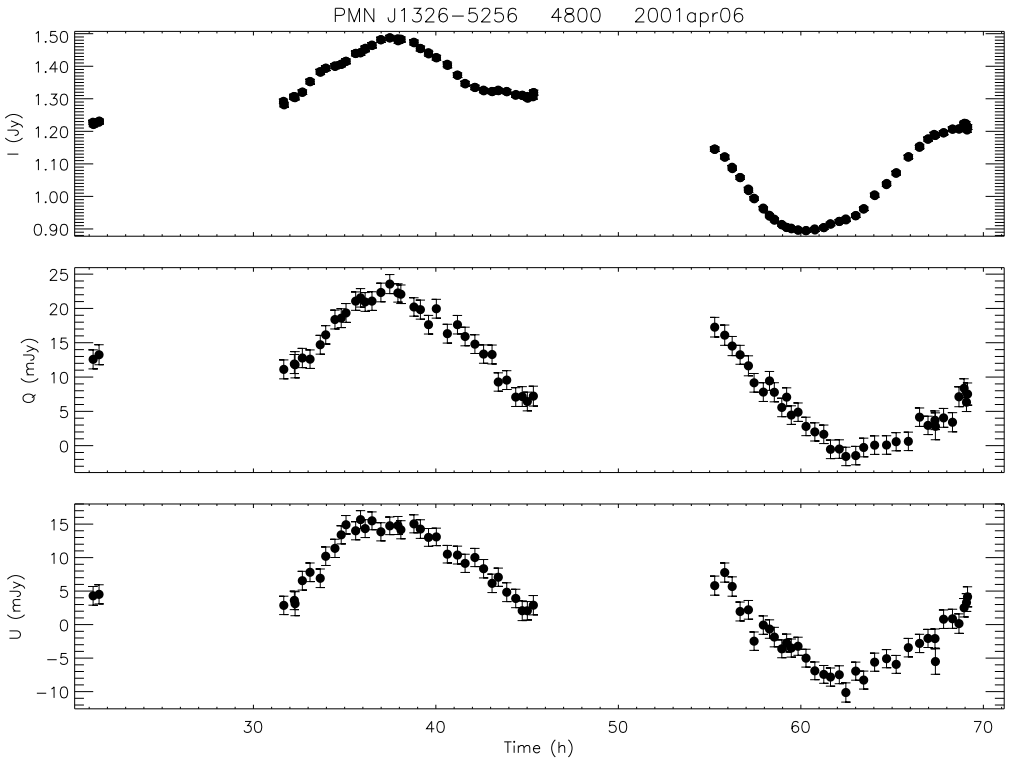

Figure 5.8: PMN J1326−5256:Stokes I, Q and U data at 4.8 GHz from the observation starting on 2001 April 6.

5.7.3 PMN J1326−5256

PMN J1326−5256 showed the largest amplitude IDV observed in any source during the ATCA monitoring program, although significant IDV was not observed in every epoch. Figure 5.8 shows data from the observation starting on 2001 April 6, at 4.8 GHz. The variability in linearly polarized flux density in this source was usually observed to be strongly correlated with variability in total flux density, suggesting that the scintillating linearly polarized component is much the same size as, and coincident with, the unpolarized scintillating component. The long term behaviour shown in Figure 5.9, however, suggests that there may be long-term intrinsic changes occurring in the source, which could complicate modelling of the polarized structure.

5.7.4 PKS 1519−273

Discovered in the ATCA IDV Survey (Kedziora-Chudczer et al., 2001b), PKS 1519−273 is an intriguing source because of its long-lived intraday variability and its usually high fractional circular polarization (CP). Macquart et al. (2000) proposed a simple model for the source based on the strong observed correlation between the variations in Stokes I and Stokes V, although the origin of the high level of CP could not be explained by any simple mechanism. More recent data suggest that there may in fact be more

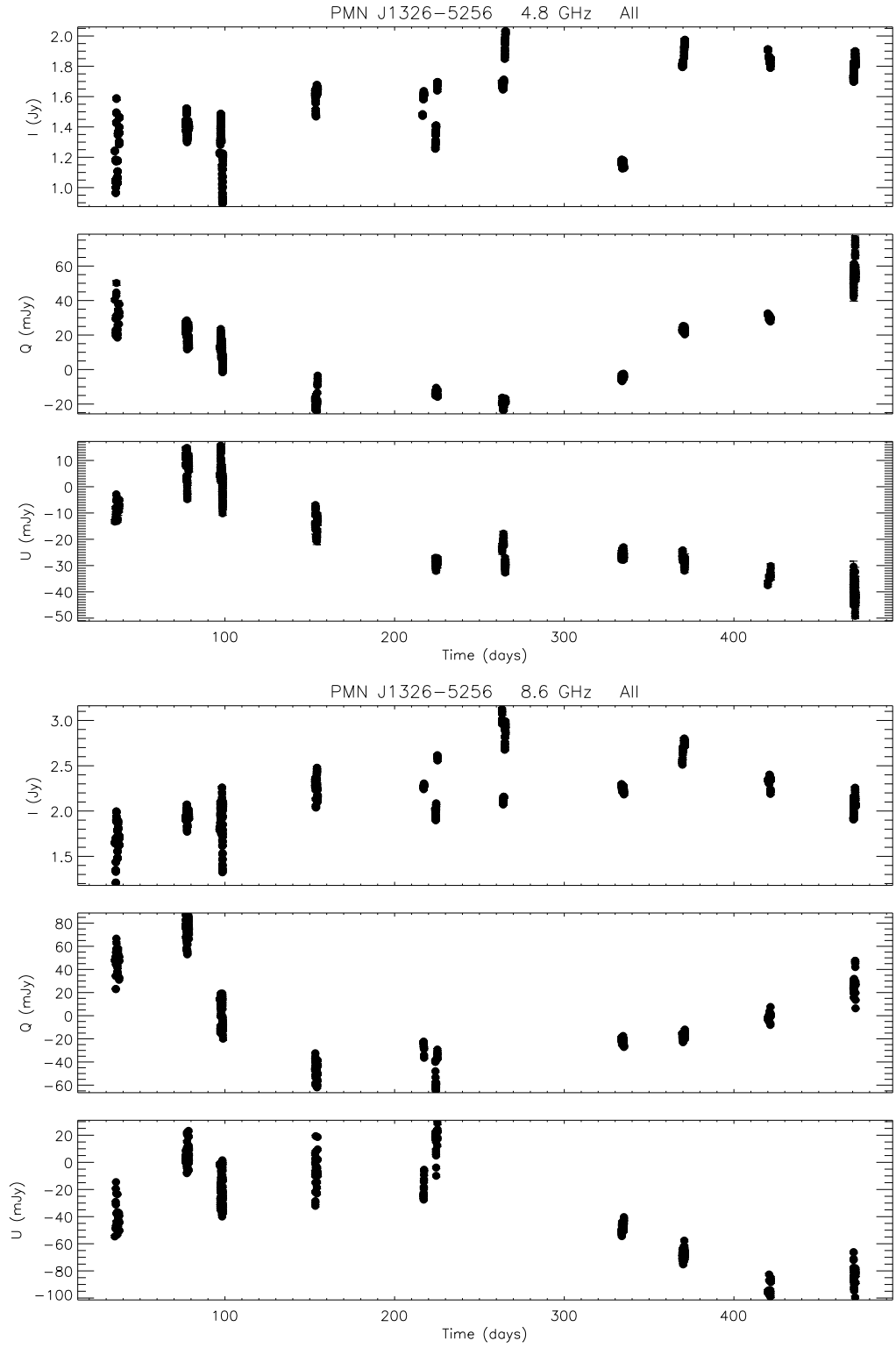

Figure 5.9: PMN J1326−5256: Stokes I, Q and U data at 4.8 and 8.6 GHz from all epochs. Day 0 in this plot is Jan 1, 2001. The data shown in Figure 5.8 start on day 96.

complex structure in the CP than the single-component model proposed by Macquart et al. (2000), which fitted data collected over 5 days in 1998 September. A detailed analysis of this source, including the data from the present monitoring program as well as data collected earlier, will be presented in a separate paper (H. Johnston et al. 2003, in prep.).

Figure 5.10 shows an example of the IDV in all four Stokes parameters for PKS 1519−273. Stokes Q and U are also shown in their alternative representations, linearly polarized flux density p and position angle of the electric vector of linear polarization. This sort of quasi-sinusoidal variability, with time-scale on the order of a day, is typical for PKS 1519−273. Figure 5.11 presents the combined data from all epochs on this source, and shows that the IDV totally dominates the observed variability - any underlying long-term trends are not obvious.

Comparing these measurements with earlier data from the ATCA blazar monitoring program (Chapter 3) and other previous observations of PKS 1519−273 (Kedziora-Chudczer et al., 2001b; Macquart et al., 2000), there is some evidence that the source has become $\sim 15\%$ brighter at 8.6 GHz over a period of several years. During the C639 monitoring program, the average flux density at 8.6 GHz was 1.7 Jy, as shown in Table 3.3, while during the present C927 program, the average 8.6 GHz flux density was 2.0 Jy. Average 8.6 GHz flux densities measured in 1994 May and August during the ATCA IDV Survey were 1.4 Jy and 1.8 Jy in each epoch respectively (Kedziora-Chudczer et al., 2001b). The lower average flux density in 1994 May could be simply a result of sampling a minimum in the scintillation pattern. The different average flux densities at 8.6 GHz for each of the longer monitoring programs, however, is more significant, as many measurements contribute to each average. The change at 4.8 GHz is much smaller, with the average 4.8 GHz flux density for the C639 program (Table 3.3) being 1.7 Jy, and for the C927 program, 1.8 Jy. The average 4.8 GHz flux densities in 1994 were 1.4 Jy (May) and 1.7 Jy (August) (Kedziora-Chudczer et al., 2001b). Certainly there is no evidence for any dramatic intrinsic changes in PKS 1519−273 over the past decade.

5.7.5 PKS 1622−253

IDV in PKS 1622−253 was discovered during the blazar monitoring program presented in Chapter 3. Figure 5.12 shows data at 4.8 GHz from two days beginning on April 6, 2001. This source typically shows changes of up to 30% in total flux density on time-scales of $\sim 1 - 2$ days. Figure 5.13 shows all the data at both frequencies. The scintillation of PKS 1622−253 has implications for modelling of longer term intrinsic outbursts, since there are large uncertainties in the underlying intrinsic flux density measured from a short observation, as was the case for the long-term monitoring data presented in Chapters 3 and 4.

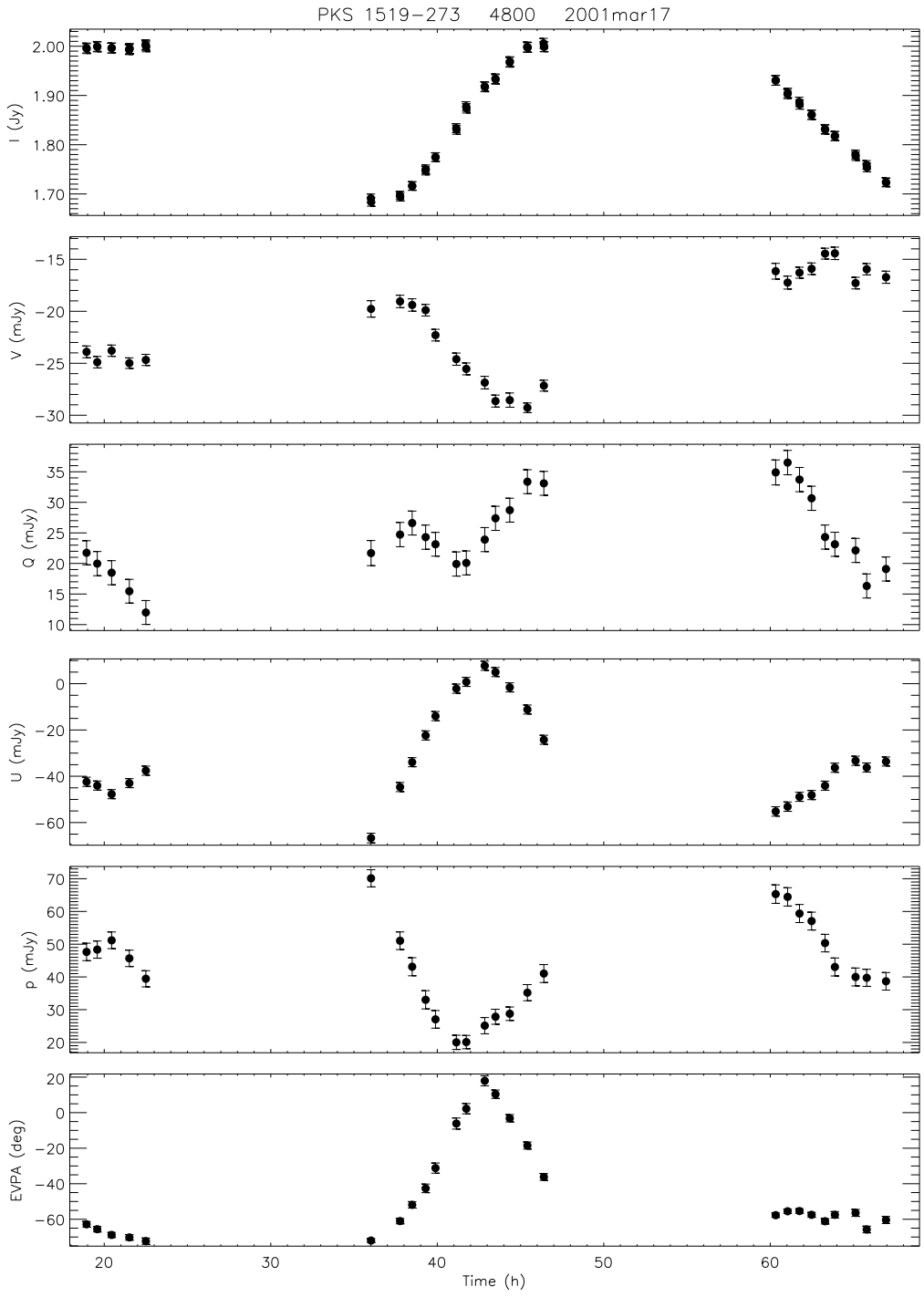

Figure 5.10: PKS 1519−273 data at 4.8 GHz from the observation starting on 2001 March 17. All four Stokes parameters I, V, Q and U are shown, as well as the equivalent representations of Q and U as linearly polarized intensity p and position angle (EVPA).

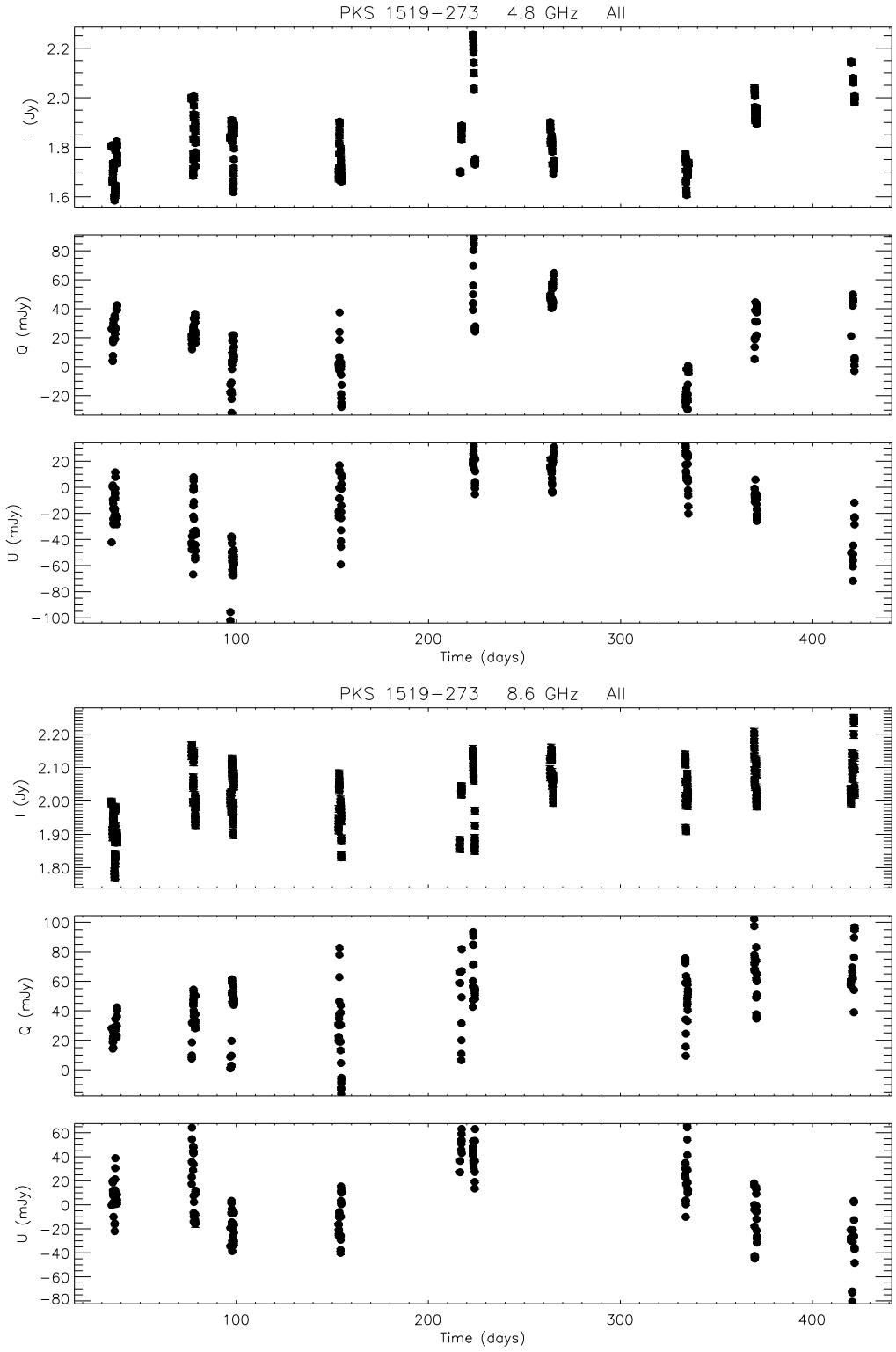

Figure 5.11: PKS 1519−273: Stokes I, Q and U data at 4.8 and 8.6 GHz from all epochs. Day 0 in this plot is Jan 1, 2001. The data shown in Figure 5.10 start on day 76.

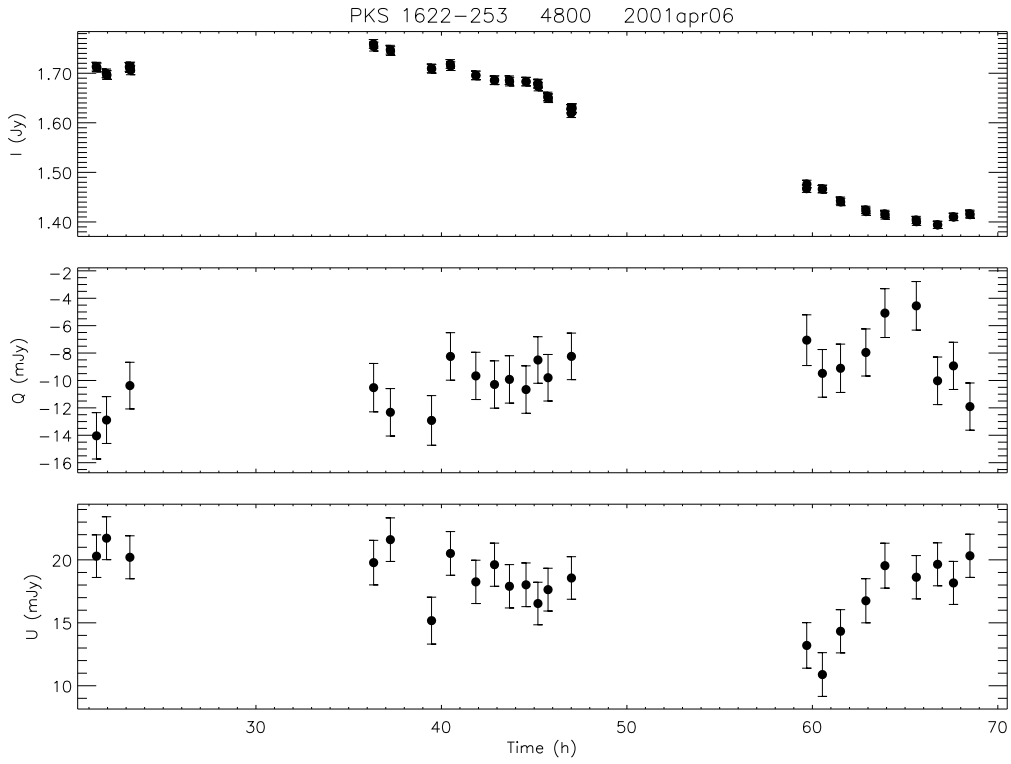

Figure 5.12: PKS 1622−253: Stokes I, Q and U data at 4.8 GHz from the observation starting on 2001 April 6.

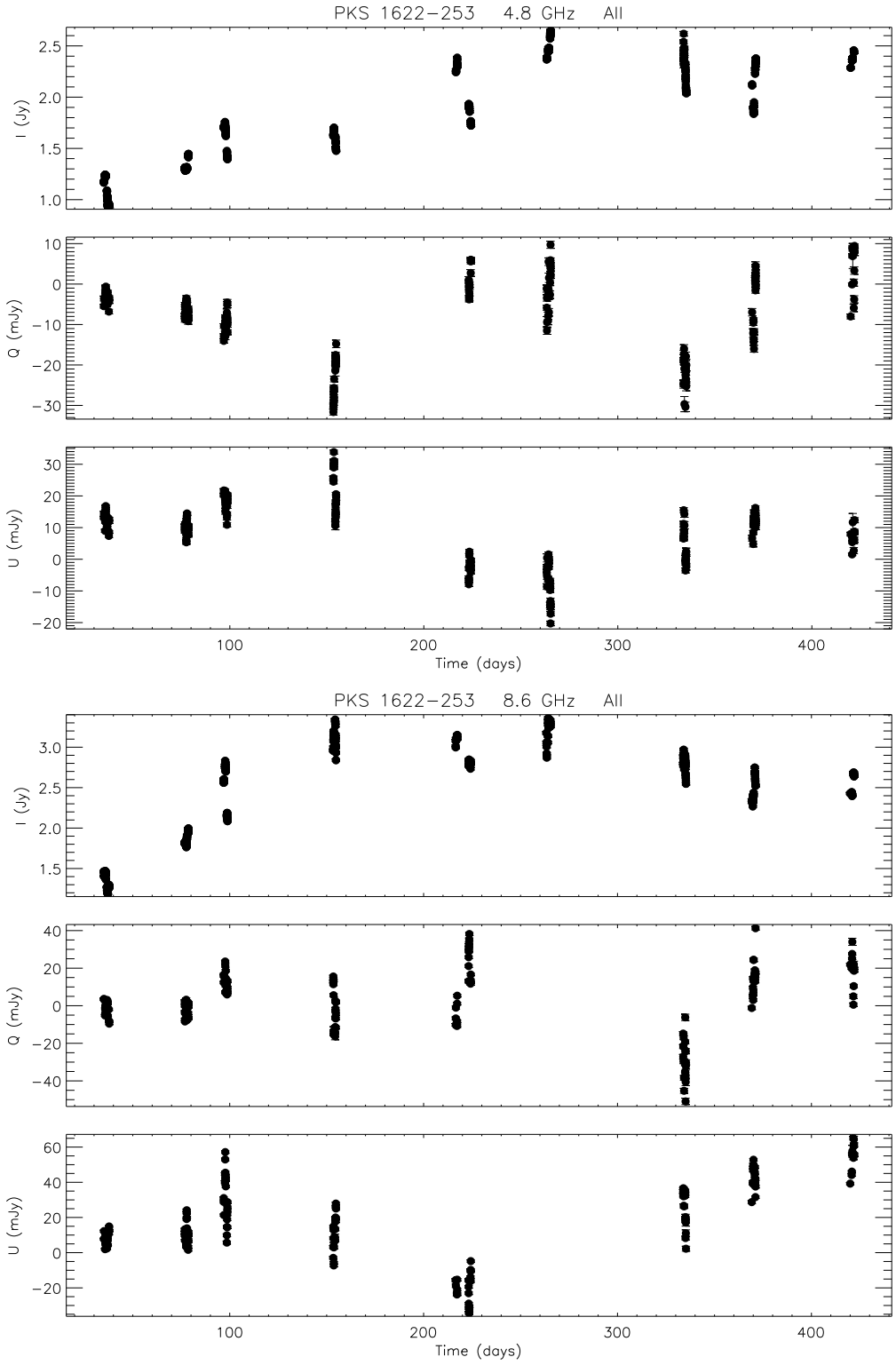

Figure 5.13: PKS 1622−253: Stokes I, Q and U data at 4.8 and 8.6 GHz from all epochs. Day 0 in this plot is Jan 1, 2001. The data shown in Figure 5.12 start on day 96.

5.7.6 PKS 0405−385: "the lion sleeps"[1]

It is interesting to note that no IDV was observed in PKS 0405−385 during the present monitoring program. The source showed only a steady, $\sim 25\%$ increase in flux density over the year (Figure 5.14). The data from 1996 presented by Kedziora-Chudczer et al. (1997) showed the flux density of PKS 0405−385 to be varying by as much as 1 Jy in an hour. The underlying cause of the short-lived outbursts of dramatic scintillation in this source is yet to be determined.

5.8 Discussion

The first results from a year-long ATCA monitoring program for IDV sources have been presented in this chapter. There is much further analysis to be done for a number of the individual sources observed. Accurate polarimetric calibration was a priority for these observations. Information on polarized substructure in the sources can be obtained from a comparison of the scintillation patterns for total intensity (Stokes I) and Stokes Q and U, and in cases where significant circular polarization is detected, Stokes V. For most IDV sources which have characteristic time-scales on the order of a day, there are large uncertainties in estimates of the time-scale from only two days of data. Detailed analysis of the *annual cycle* is presented here only for PKS 1257−326 (see Chapter 6), which had by far the shortest characteristic time-scale of any source observed. Many scintillating sources also show significant intrinsic variability, which may influence the observed scintillation patterns and annual cycle behaviour.

[1]From the song known as "Wimoweh", and later as "The Lion Sleeps Tonight". First version was written and recorded in 1939 by Zulu singer and entertainer Solomon Linda, who titled the song "Mbube," which is Zulu for "The Lion."

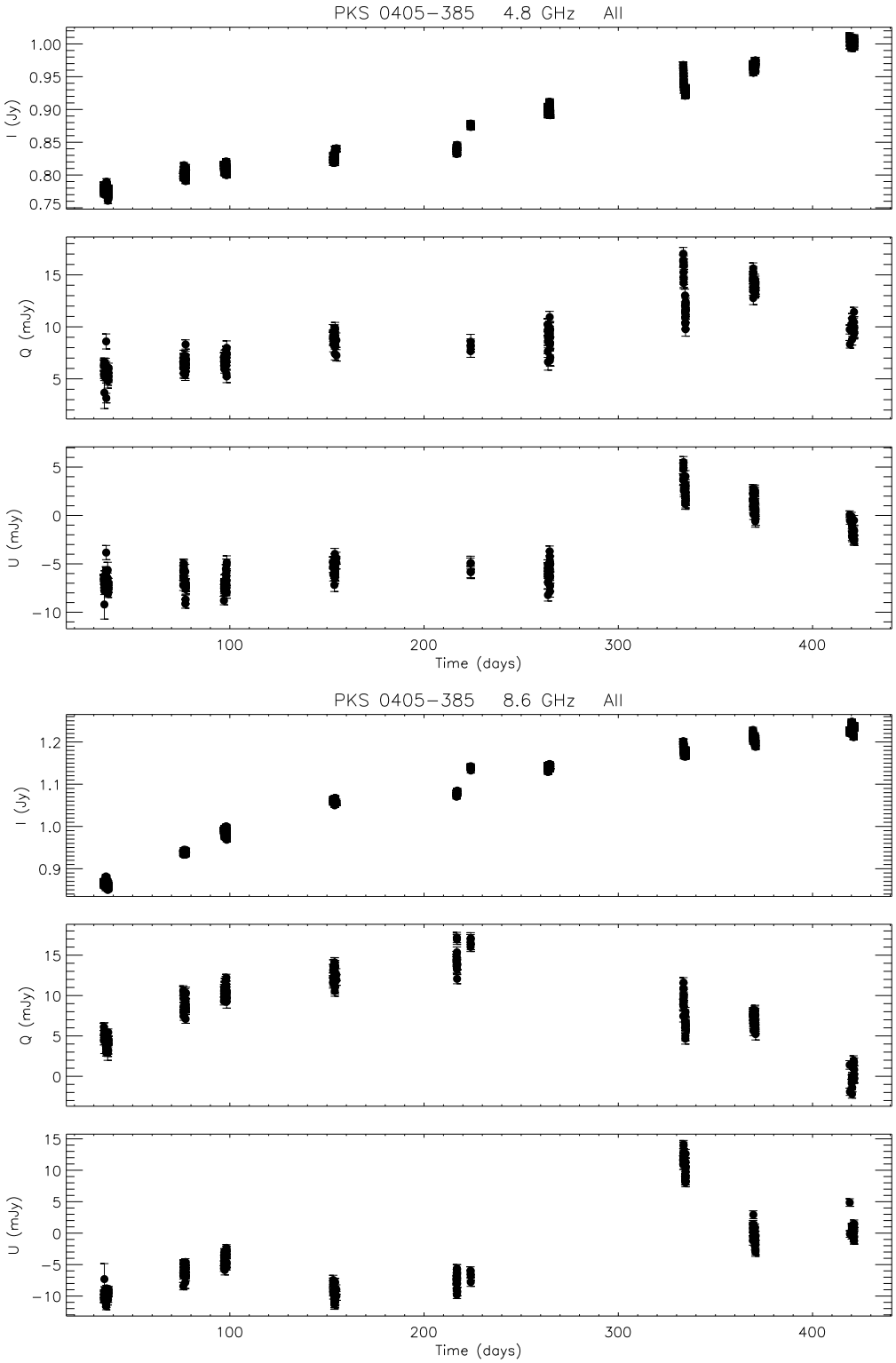

Figure 5.14: PKS 0405−385: Stokes I, Q and U data at 4.8 and 8.6 GHz from all epochs. Day 0 in this plot is Jan 1, 2001.